Energy & Buildings 247 (2021) 111114

Contents lists available at ScienceDirect

Energy & Buildings

journal homepage: www.elsevier.com/locate/enb

Building energy and thermo-hydraulic simulation (BETHS) for district heat system in residential communities: A case of Shenyang, China

Jianxiang Huang [a,c,*], Yi Xu [a,b], Phil Jones [d], Xiaojun Li [d,e], Mengdi Guo [a,b], Gang Liu [b], John S. Ji [f,g]

[a] Department of Urban Planning and Design, 8/F Knowles Building, The University of Hong Kong, Pokfulam Road, China Hong Kong Special Administrative Region
[b] School of Architecture, Tianjin University, No. 92 Weijin Road, Nankai District, Tianjin, China
[c] The University of Hong Kong Shenzhen Institute of Research and Innovation, 5/F, Key Laboratory Platform Building, Shenzhen Virtual University Park, No.6, Yuexing 2nd Rd, Nanshan, Shenzhen, China
[d] Welsh School of Architecture, Cardiff University, King Edward VII Avenue, Cardiff CF10 3NB, UK
[e] School of Architecture, Hunan University, Yuelu district, Changsha, Hunan Province, China
[f] The Environmental Research Center, Duke Kunshan University, Academic Building 1079, Kunshan, Jiangsu Province, China
[g] Global Health Research Center, Duke Kunshan University, No. 8 Duke Avenue, Kunshan, Jiangsu, China

ARTICLE INFO

Article history:
Received 16 October 2020
Revised 3 April 2021
Accepted 11 May 2021
Available online 21 May 2021

Keywords:
District heating
Thermo-hydraulic modelling
Building performance simulation
Energy conservation

ABSTRACT

District Heating Systems (DHS) have received renewed attention in relation to their environmental, economic, and health benefits. Research literature on DHS tends to focus separately, either on the thermo-hydrological modelling or building energy demand. Rarely are there combined simulation approaches that consider the interactions between the district heating system and the buildings they serve. There is a practical need for a coupled simulation model to inform operation and energy retrofit strategies, such as, building insulation, water leakage prevention, and achieving comfortable indoor air temperatures. In this study, a novel simulation model, BETHS, is developed to predict the time-varying energy performance and occupant thermal comfort of a cluster of buildings served by a DHS in the urban context. The simulation results are compared with field measurement data collected for a secondary network consisting of 12 buildings and 2788 m of pipeline network over a 10-day period, in Shenyang, Liaoning, China. Predicted water temperature and indoor air temperature showed reasonable agreements with measured data. Simulation results suggested an energy saving of 35% for improved building insulation, 32% for switching from coal to gas, 18% for reduced indoor temperature, 14% for water leakage prevention, and 67% if all are combined. The BETHS model can be a valuable extension to a building energy simulation framework, and support retrofit strategies and operational decisions for existing DHS networks.

1. Introduction

1.1. Background

A District Heating System (DHS) distributes thermal energy in the form of hot water or steam from a central source to residential, commercial or industrial consumers [1]. DHS is considered an energy efficient heating solution, offering economic, environmental, and health benefits [2]. Compared with distributed heating systems in individual buildings, the DHS can reduce carbon emissions, save energy, and enhance human health by reducing air pollutants such as sulphur oxides (SOx), nitrogen oxides (NOx), and particulate matter (PM), in additional to providing affordable warmth in properly heated buildings. Estimates of the total number of DHS installed globally are around 80,000 [3] (Fig. 1) and rising, driven primarily by the aforementioned benefits.

A large number of DHS were installed in Northern China, with up to 3 million kilometres of pipeline length serving some 7 billion square meters of building floor area, according to the official estimates [4]. A majority of these types of systems rely on coal as the source of heat input [5]ing and adopteing a fixed flow design, in which the water flow within the pipelines cannot be easily adjusted to suit the dynamic heating needs, leading to uneven indoor air temperatures and inefficiencies in energy use [6]. Driven by environmental protection plans, the central government has proposed plans to convert 70% of households in Northern China from coal-based heating systems to those based on natural gas,

* Corresponding author at: Department of Urban Planning and Design, The University of Hong Kong, 8/F Knowles Building, Pokfulam Road, Hong Kong SAR, China.
E-mail address: jxhuang@hku.hk (J. Huang).

https://doi.org/10.1016/j.enbuild.2021.111114
0378-7788/

Nomenclature

List of Symbols

Symbol	Explanation (Unit)
dt	A sufficiently small time step (s)
M_k	Mass of the wall k (kg)
$V_{i,j}$	Water flow rate from node i to j (kg/s)
V_S	Water flow rate at the supply mixer (kg/s)
$\overline{V}_S$	Mean water flow rate at the supply mixer (kg/s)
V_T	Rate of water leakage top-up (kg/s)
$\overline{V}_T$	Mean rate of water leakage top-up (kg/s)
m_i^{leak}	Water leakage rate at node i (kg/s)
ρ_{air}	Density of air (kg/m^3)
ρ_w	Density of water (kg/m^3)
e	Absolute roughness of pipe wall (m)
L_{ij}	Length of pipeline between node i and j (m)
D_{ij}	Inner diameter of pipeline between node i and j (m)
r_1	Inner radius of a pipe (m)
r_2	Outer radius of a pipe (m)
r_3	Pipe radius with insulation layer (m)
A_{ij}	Area of the pipe section connecting i and j (m^2)
A_k	Surface area of the wall k (m^2)
V_{unit}	Volume of the residential unit (m^3)
P_i	Water pressure at node i (Pa)
P_j	Water pressure at node j (Pa)
P_S	Water pressure at the supply mixer (Pa)
P_R	Water pressure at the return outlet (Pa)
H_p	Pressure head at the circulator pump (Pa)
ΔP_{ij}^{fri}	Friction-induced pressure drop between node i and j (Pa)
ΔP_{ij}^{fit}	Fitting-induced pressure drop between node i and j (Pa)
T_k^{mrt}	Mean radiant temperature of building external surface k (K)
T_k^{surf}	Temperature of building external surface k(K)
T_{soil}	Temperature of the ground soil at the depth of 1.6 m (K)
dT_i	Change of temperature between time steps (K)
T_j	Water temperature at node j(K)
T_i	Water temperature at node i (K)
T_S	Water temperature at the supply mixer (K)
T_R	Water temperature at the return outlet (K)
T_M	Temperature of the top-up water (K)
T_{ind}	Indoor air temperature in a residential unit (K)
T_{out}	Outdoor air temperature of the ambient environment (K)
R_1	Thermal resistance from the center of pipe to its periphery (K/W)
R_2	Thermal resistance of the pipe wall (K/W)
R_3	Thermal resistance of the insulation layer (K/W)
C_a	Specific heat capacity of air (J/kg.K)
C_w	Specific heat capacity of water (J/kg.K)
C_k	Specific heat capacity of wall surface (J/kg.K)
Q_{ij}^{rad}	Radiative heat loss to a building between node i and j (W)
q_{ij}	Fluid internal heat gain (W)
Q_{ij}^{loss}	Conductive heat loss to the ground between node i and j (W)
Q_{ex}	Rate of heat gains from the heat exchanger (W)
Q_b	Rate of heating energy supplied to buildings (W)
Q_{in}	Sum of internal heat gains from lighting, people, and electric appliances (W)
E_p	Rate of energy gains from the circulator pump (W)
E_{total}	Rate of total energy inputs for the district heating system (W)
E_k	Incident solar radiation at surface k W/m^2
E_g	Normal solar irradiance at the glazing g (W/m^2)
k_w	Thermal conductivity of water (W/m^{2}K)
k_p	Thermal conductivity of the pipe wall (W/m^{2}K)
k_i	Thermal conductivity of the insulation layer (W/m^{2}K)
h_k	Convective heat transfer coefficient from the wall surface to the air (W/m^{2}K)
h_{rad}	Heat transfer coefficient of the radiant floor emitter (W/m^{2}K)
U_k	U-value of the wall k (W/m^{2}K)
σ	Stephan-Boltzmann's constant (W/m^{2}K)
ACPH	Number of air changes per hour (count)
G	Number of glazings in a residential unit (count)
J	Number of nodes in the DHS network (count)
K	Number of wall surfaces in a residential unit (count)
N	Number of nodes in the DHS pipeline network (count)
η	Overall efficiency of the secondary DHS network (ratio)
S_g	Solar factor (G-value) of the glazing g (ratio)
α_k	Solar absorption coefficient of the surface material (ratio)
ε_k	Surface emissivity of the wall k (ratio)
f_{ij}	Friction factor of pipeline between node i and j (dimensionless)
Re	Reynolds number of waterflow inside pipelines (dimensionless)
K_{ij}	Size-dependent pressure loss coefficient for the pipe fitting between node i and j (dimensionless)

geothermal, solar or wind power by 2021 [4]. Meanwhile, building energy retrofit, especially the improvement of the insulation of walls and windows, have been practiced widely in Northern China [7,8].

A large body of research literature on Chinese DHS has emerged in recent years [12]; the majority are divided into 1) district heating pipelines and 2) building energy models. Rarely are these two components combined in the modelling literature. There is a practical need for a reliable simulation tool to predict the operating energy demand of district heating pipelines, combined with the energy performance and thermal conditions of the buildings.

The aim of this study is two-fold: 1) to develop and evaluate a novel simulation model to predict the time-varying energy performance of buildings connected to district heating systems; 2) to test the model in relation to its usefulness for informing operational and retrofit strategies by predicting energy savings and greenhouse gas emissions. A physics-based model has been developed to simulate the time-varying network flow characteristics, building indoor temperature and system efficiency on an hourly basis. Simulation results have been evaluated against field measurement data collected in Shenyang in Northern China. Sensitivity. Studies were then conducted to predict energy savings potential under various retrofit strategies for the types of DHS network commonly found in Northern China.

1.2. Relevant works

Two bodies of research literature focus on 1) the district heating system and 2) building energy performance. Rarely are there coupled simulation models that can account for the time-varying energy performances of buildings and occupant thermal comfort for a cluster of buildings served by DHS in an urban context.

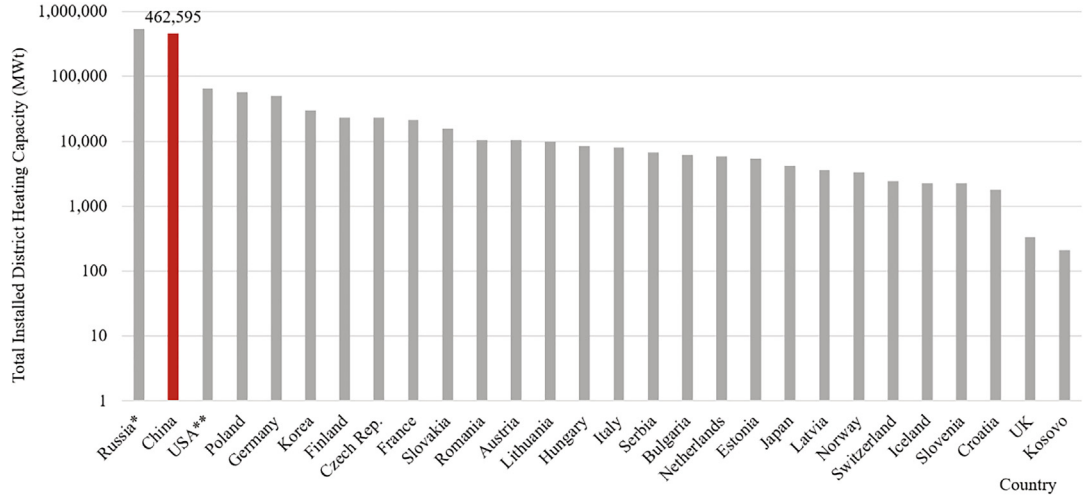

Fig. 1. Total installed district heating capacity by country. Data Source: Euro Heat & Power, 2015 [9] * Data for Russia from DBDH estimates in 2013 [10] ** Data for USA from EIA estimates in 2018[11]

1.2.1. Thermo-Hydraulic models

Current DHS models generally divide a DHS network into pipes, nodes and buildings [13], to solve for hydraulic flow, pressure and heat transfer using thermo-hydraulic equations [14]. Numerical minimization methods were developed to solve the model equations, including the Hardy-Cross method, the linear theory method [15], and the Newton-Raphson method [16,17] which combine the nodal head and loop equation methods [14]. Several commercial software tools have been developed based on the above simulation methods. Examples include the Heating and Air Conditioning Piping Simulation and Analysis Toolkit (HACNet) developed by Fu et al. [18] and HEATSPOT developed by Knutsson et al. [19]. Most models treat a building as a standardized heat load, which limits their capacity to predict the dynamic energy performance for an urban community connected to district heating systems. A major limitation of these types of models lies in the uncertainties in assessing the energy use of the entire district, especially in a large DHS system of considerable heterogeneity of heating loads among buildings [20].

1.2.2. Building energy models

Many physics-based models have been developed to simulate the thermal performance of individual buildings. Examples such as HTB2 [21], EnergyPlus [22] and TRNSYS [23] which have been applied extensively in research and practice to evaluate building performances. These models have been later extended to assess the performance of a group of buildings, notable studies include Virvil [24], UMI[25], and CitySim[26]. To inform the thermal boundary conditions of individual buildings in an urban context, multizone models and CFD methods were used to assess airflow and temperature fields between buildings [27–29], although such models were initially developed for indoor spaces in large buildings [30,28,31]. Aside from physics-based models, there are also historical methods, such as heating degree day (HDD), to estimate the approximate heat loss through building fabrics [32]. Other approaches include regression [33], times series neural network prediction [34] and artificial intelligence [35].

1.2.3. Research gaps

Despite the abundance of literature on the above two categories, there are no coupled simulation models that can account for the time-varying energy performances and occupant thermal comfort for a cluster of buildings served by DHS in an urban context. As a result, the energy demand profiles of buildings have usually been treated as a constant per unit heating area [36], which may exhibit considerable uncertainties when applied to the dynamic simulation of a residential community, where space occupancy and external weather conditions vary by the hour. The lack of reliable prediction of heating demand is considered a key barrier in the optimization of DHS systems [37]. For this reason, the design of DHS rarely takes into account the load heterogeneity of buildings over time [38].

Due to the interactive nature of building heating demand and the operation of a DHS network, there is a need for a coupled model for DHS pipeline network and buildings. Such a model enables a "whole system" approach, which can inform the thermal design of buildings in consideration for the capacity of DHS in order to deliver sufficient heating for occupant comfort and health. The model can then serve as an important tool for energy retrofits of existing systems, or the design of new systems. The coupled model allows the comparison of energy-saving potentials for alternatives in design, operation and retrofitting, which is essential in setting priorities in decision-making in reference to the "design significance" concept coined by Guillen et al. [39]

2. Methods

The Building Energy and Thermo-Hydraulic Simulation (BETHS) was developed to describe the water flow velocity, pressure, and temperature profiles in a DHS network and the indoor thermal conditions of buildings. The performance of the BETHS model was evaluated using field studies conducted in Shenyang in Northern China. The BETHS model was used to assess energy savings and carbon emission reductions for various strategies such as improving building insulation, switching from coal to gas, reducing indoor temperature, and water leakage prevention.

2.1. Building energy and Thermo-Hydraulic model

The BETHS model followed the 4-step workflow: 1) to calculate water flow velocities and pressure drop across the DHS pipeline network; 2) to compute the temperature profile for the supply

water at buildings; 3) to calculate pipeline heat losses to the buildings via radiant floor heating and the return water temperature; 4) to calculate energy intensity and DHS system efficiency. A schematic depiction of the model is described in Fig. 2; details for each step are specified below.

A thermo-hydraulic flow network model was developed to simulate the flowrate and temperature within a water-based DHS pipeline network and the indoor thermal conditions in the heated buildings. A nodal approach was adopted, assuming that the pipeline network can be subdivided into a finite number of interconnected nodes including the heat source, conduits, and radiant floor emitters inside buildings. A homogeneous pressure (P_i), temperature (T_i), and density ρ_w were assumed for a node i at each time step. Inter-nodal flows are governed by pressure differences, pipe fittings, openings, control valves. For fluid flows within the pipeline network, Mass Conservation, Pressure Balance, and Energy Conservation equations apply, as it is specified by the ASHRAE handbook [40].

2.1.1. Network flow & pressure

The aim was to compute pressure drops and flow velocity across the pipeline network. The input parameters were pressure head at the circulator pump and pipeline parameters. Two sets of equations were used: Mass Conservation and Pressure Balance.

Mass conservation, alternatively known as mass continuity, is expressed as the sum of water inflow and outflow via each node i equals to zero (Formula (1))

$$0 = \sum_{i=1}^{i=N} V_{ij} - m_i^{leak} \tag{1}$$

where $V_{i,j}$ is the water flow rate from node i to j; m_i^{leak} is the rate of water leakage at node i, if any; N is the number of nodes in the DHS network.

Pressure balance is derived from the Bernoulli Equation in which the sum of kinetic, potential, and internal energy of a fluid along the streamline stays constant [40]. As it is expressed in Formula (2), for a steady pipe flow between node i and j, the pressure difference P_i - P_j equals the sum of the friction-induced pressure drop (ΔP_{ij}^{fri}) and fitting-induced pressure drop (ΔP_{ij}^{fit}).

$$P_i - P_j = \Delta P_{ij}^{fri} + \Delta P_{ij}^{fit} \tag{2}$$

The friction-induced pressure drop ΔP_{ij}^{fri} is expressed by the Darcy–Weisbach Equation [40], in which ΔP_{ij}^{fri} is a function of water density ρ_w, flow velocity V_{ij}, pipeline length L_{ij}, pipe inner diameter D_{ij}, and the Friction Factor f_{ij} along the pipe node i and j (Formula (3)).

$$\Delta P_{ij}^{fri} = \frac{\rho_w {V_{ij}}^2}{2} \frac{L_{ij}}{D_{ij}} f_{ij} \tag{3}$$

The Friction Factor f_{ij} is expressed by the Colebrook equation [41] as a function of pipe roughness e, pipe inner diameter D_{ij}, and the Reynolds number Re of waterflow inside pipelines (Formula (4)). This formula applies for the study condition of turbulent water flow, in which Re > 4,000.

$$\frac{1}{\sqrt{f_{ij}}} = -2log_{10}\left[\frac{e}{3.7D_{ij}} + \frac{2.51}{Re\sqrt{f_{ij}}}\right] \tag{4}$$

The fitting-induced pressure drop ΔP_{ij}^{fit} from i to j is caused by pipe fittings such as control valves or pipe elbows. ΔP_{ij}^{fit} was expressed in Formula (5) as a function of the flow velocity V_{ij}, water density ρ_w, geometry and size-dependent pressure loss coefficient K_{ij} listed by ASHRAE handbook [40] for each type of pipe fitting.

$$\Delta P_{ij}^{fit} = \frac{{V_{ij}}^2}{2} \rho_w K_{ij} \tag{5}$$

The Mass Conservation and Pressure Balance equation sets were solved numerically using the Python programming language. Input parameters and constants are written into matrices for the specified simulation case. The outputs were the flow velocity and pressure parameters across the DHS pipeline network.

2.1.2. Temperature of water supply at buildings

The aim is to calculate the water temperature along the DHS network which supplies buildings (end user). The inputs are the supply water temperature at the district heating substation, which is taken from measured data. Temperatures of the hot water supply at each building are calculated using energy conservation and the Bernoulli equation.

Energy conservation is assumed for each pipe node, in which the sum of heat gains/losses via fluid exchange, conductive heat loss to the ground, radiative heat loss to buildings, thermal massing effect, and internal heat gains equals zero, as it is expressed in Formula (6):

$$0 = \sum_{i=1}^{i=J} (V_{ji}\rho_w(T_j - T_i)) - \rho_w V_{ij} C_w \frac{dT_i}{dt} + q_{ij} - Q_{ij}^{loss} - Q_{ij}^{rad} \tag{6}$$

where T_j and T_i are water temperature at node j and i respectively; C_w is the specific heat capacity of water; dt is a sufficiently small time step (s), dT_i is the temperature change between two time steps

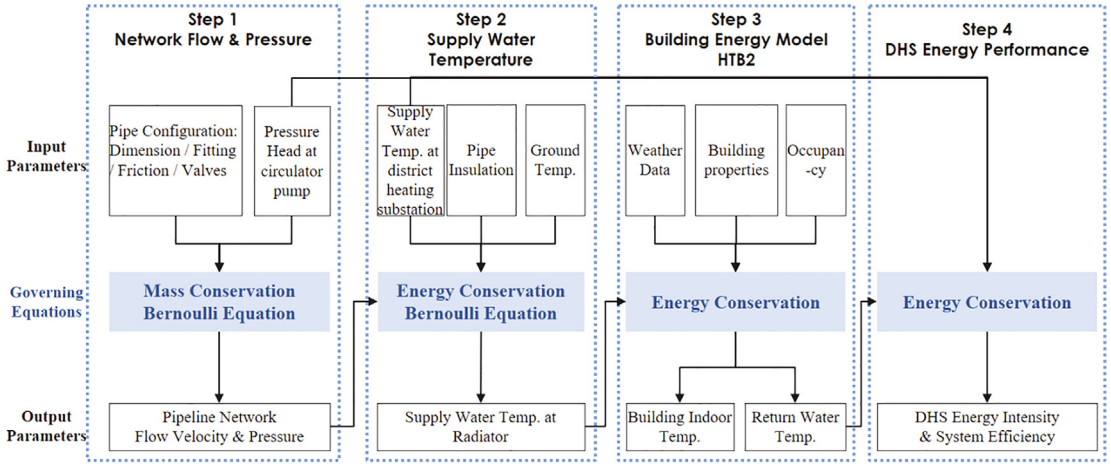

Fig. 2. A schematic depiction of the workflow of the BETHS model.

(K); q_{ij} is the fluid internal heat gain; $Q_{ij}^{loss}$is the conductive heat loss to the ground; Q_{ij}^{rad} is the radiative heat loss to a building.

The rate of fluid internal heat gains q_{ij} between node i to j from friction and resistance of pipeline fitting is expressed in formula (7). Changes of fluid potential energy is negligible in flat terrain, such as it is the case in our study.

$$q_{ij} = \left(\Delta P_{ij}^{fri} + \Delta P_{ij}^{con}\right) A_{ij} V_{ij} \tag{7}$$

The rate of pipeline heat loss Q_{ij}^{loss} (W) is governed by the thermal resistance of the water, pipe wall, and the insulation layer, which can be expressed by Fig. 3 as a function of mean water temperature of the pipe node ($\frac{T_i+T_j}{2}$), the mean temperature of the ground soil T_{soil}, and the thermal resistance of the pipe and the insulation layer R_1 to R_3 (Formula (8)) according to the ASHRAE Handbook[40]:

$$Q_{ij}^{loss} = \left(\frac{T_i + T_j}{2} - T_{soil}\right) / (R_1 + R_2 + R_3) \tag{8}$$

where R_1 is the thermal resistance from the center of pipe to its periphery and $R_1 = \frac{1}{k_w \pi r_1 L_{ij}}$, which is a function of the thermal conductivity of water k_w, pipe length L_{ij}, and the pipe inner radius r_1. R_2 is the thermal resistance of the pipe wall and $R_2 = ln(\frac{r_2}{r_1}) \ / \ 2\pi k_p L_{ij}$, which is a function of the pipe inner and outer radius, r_1 and r_2, and the thermal conductivity of pipe wall k_p(W/m^{2}K), and the pipe length L_{ij}; R_3 is the thermal resistance of the insulation layer and $R_3 = ln(\frac{r_3}{r_2}) \ / \ 2\pi k_i L_{ij}$, which is a function of the pipe radius with and without the insulation layer, r_2 and r_3, the thermal conductivity of insulation k_i, and the pipe length L_{ij}.

2.1.3. Building model (HTB2)

Building surface temperature, heating performance and indoor air temperature are dynamically modelled for buildings and apartment units connected to DHS using HTB2 [21], an advanced numerical building energy model developed at the Welsh School of Architecture at Cardiff University. HTB2 accounts for building floor plans, construction details and parameters of the radiant floor emitters [21]. HTB2 is flexible and can be easily modified to be coupled with the thermo-hydraulic DHS model developed in 2.1.1 and 2.1.2. HTB2 has been developed over fourdecades and extensively evaluated by the IEA Annex 1 [42], IEA task 12 [43] and the IEA BESTEST [44]. The input data are hourly on-site weather data, occupancy, flowrate and temperature of water through the pipes embedded in the radiant floor. The outputs are hourly indoor air temperature for each residential unit, heat output from radiant floor emitters, and return water temperature to DHS.

For the pipeline between nodes i to j that passes through a building radiant floor and discharges heat to the indoor spaces, the heat supplied to a building Q_{ij}^{rad} is governed by the heat transfer coefficient of the radiant floor emitter h_{rad}, the length of the pipe L_{ij}, the mean water temperature at the radiant floor emitter $(T_i + T_j)/2$ and the indoor air temperature T_{ind} (Formula (9))

$$Q_{ij}^{rad} = h_{rad} L_{ij} \left(\frac{T_i + T_j}{2} - T_{ind}\right) \tag{9}$$

Energy conservation was assumed for each residential unit, in which the sum of heat gains / losses from lighting, small powers, occupancy, fabric conduction, thermal massing and ventilation equals zero, as it is shown in Formula (10):

$$0 = Q_{in} - ACPH(T_{out} - T_{ind})\rho_{air} C_p V_{unit} + \rho_{air} C_a V_{unit} \frac{dT}{dt} + Q_{ij}^{rad} + \sum_{g=1}^{g=G} E_g G_g + \sum_{k=1}^{k=K} U_k A_k \left(T^{in} - T_k^{surf}\right) \tag{10}$$

where Q_{in} is the sum of internal heat gains from lighting, people, and electric appliances; ACPH is the number of air changes per hour; $(T_{out}$ - $T_{ind})$ is the temperature different between the outdoor and the indoor air; ρ_{air} is the density of the air; V_{unit} is the volume of the residential unit; C_a is the heat capacity of air, dT is the change of air temperature within a small time step dt; Q_{ij}^{rad} is the rate of heat gains from the radiant floor emitter; K and G are the numbers for surfaces and glazings in the residential unit; U_k andA_k are the U-value and the surface area of the wall k; T_{ind} is the indoor air temperature; E_g and S_g are the normal solar irradiance and the Solar Factor (G-value) of the glazing g; T_k^{surf} is the temperature of building external surface k, including walls or roofs, which can be solved by assuming energy conservation at surface among solar/long-wave radiation, convection, conduction, and thermal massing as shown in Formula (11) below.

$$0 = \alpha_k E_k + U_k \left(T_{ind} - T_k^{surf}\right) + h_k \left(T_{out} - T_k^{surf}\right) + \frac{1}{2}\varepsilon\sigma\left(T_k^{mrt4} - T_k^{surf4}\right) + \frac{dT}{dt} M_k C_k \tag{11}$$

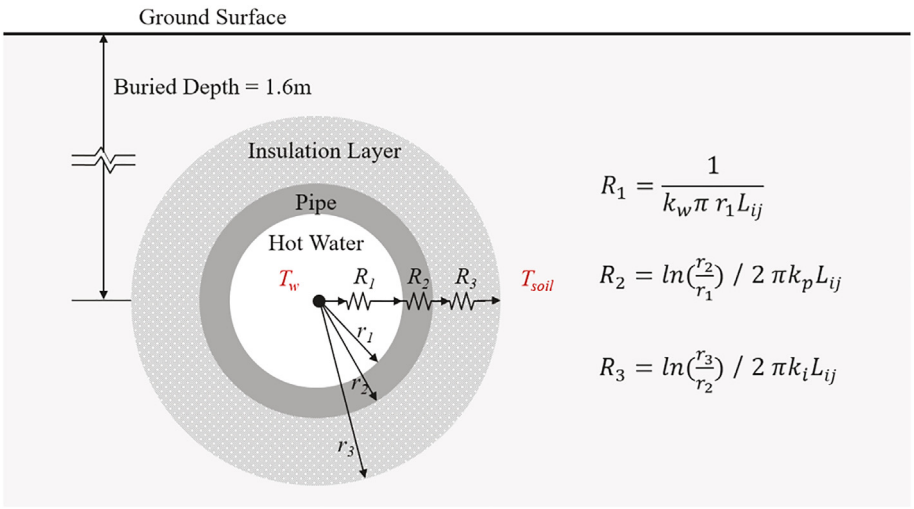

Fig. 3. A schematic depiction of the radial conductive heat loss through the hot water pipe with insulation.

where E_k is the incident solar radiation at surface k calculated using HTB2; α_k is the solar absorption coefficient of the surface material; U_k is the heat transmission coefficient of the wall k; T_{ind} is indoor temperature inside the building; h_k is the convective heat transfer coefficient from the wall surface to the air; T_{out} is the outdoor air temperature; ε_k and σ are the surface emissivity and Stephan-Boltzmann's constant; T_k^{mrt} is the mean radiant temperature at the surface (K); $\frac{dT}{dt}$ is the surface temperature changes during each time-step; M_k and C_k are the mass and material specific heat capacity of the wall surface k. The outdoor air temperature T_{out}, surface temperature T_k^{surf}, and the return water temperature T_j can be solved using Formula (9)–(11).

2.1.4. DHS energy performance

With the flow and temperature characteristics solved for the DHS and buildings, the last step was to evaluate energy efficiency of the system (secondary DHS network). The total energy input for the DHS E_{total} included energy gains from the heat exchanger Q_{ex} and the circulator pump E_p, as it is expressed in Formula (12)

$$E_{total} = Q_{ex} + E_p \tag{12}$$

Q_{ex} is a function of temperature different between water supply and return together with compensations for water leakage, if any, as it is shown in Formula (13):

$$Q_{ex} = (T_S - T_R) * V_S * C_w + \sum_{i=1}^{i=N} m_i^{leak}(T_S - T_M \tag{13}$$

where T_S and T_R are water temperatures at the supply mixer and the return outlet respectively; $V_S$is the water flow rate at the supply mixer; m_i^{leak} is the water leakage rate at node i; T_M is the temperature of the top-up water, assumed to be the temperature of the water main; N is the total number of nodes in the DHS pipeline network;

Energy gains from the circulator pump E_p is a function of the water flow rate at the supply mixer and the total pressure loss of the hydraulic network (Formula (14)).

$$E_p = \frac{(P_S - P_R) * V_S}{\rho_w} \tag{14}$$

where P_S and P_R are the water pressure at the supply mixer and the return outlet. The overall efficiency of the DHS η can be expressed as the ratio between heating energy supplied to buildings Q_b and total energy input to the system E_{total}. η can be expressed in Formula (15) for a network of N buildings.

$$\eta = \frac{Q_b}{E_{total}} = \frac{\sum_{i=1}^{i=N} Q_{ij}^{rad}}{Q_{ex} + E_p} \tag{15}$$

2.2. Field studies

Field studies were conducted in Shenyang, Liaoning Province, China. Measurement data were collected for a residential community over a 15-day period in March 2017. Operational data were collected from 51 DHS substations during the heating season of 2016–17. The aim was to evaluate the simulation results from BETHS, and to provide an empirical estimate of DHS performance.

2.2.1. Climate and site

Shenyang (N41°48′, E123°27′) is the provincial capital city of the Liaoning Province in Northern China. The city features a cold climate, with a monthly mean temperature in January of −11.0℃ [45]. Heating is provided during the officially designated heating season between November 1 and March 31. 70% of the city's building stocks are served by DHS [46], the majority of the systems (51%) rely on coal-fired boilers as heating sources; a minority of the systems (36%) use Combined Heat and Power (CHP); the remaining 12% use geo-thermal, natural gas, electricity or solar sources [47].

Field measurement was conducted at the Central University Town (CUT) located in the Shenbei New Area, 15 km north of Shenyang's city centre (Fig. 4). CUT was representative of the city's residential communities in scale, density and building types, consisted of 56 residential buildings, 44 slab buildings that are 6-storey (B1-15, C1-14, and E1-15), and 12 high-rise towers that are 18 storeys (A1-6) and 12 storeys (D1-6) respectively. The CUT community comprised 4,335 residential units. It was built and fully occupied since 2011 and accommodates some 13,000 people.

The spatial configuration and the layout the secondary DHS networks in the CUT community is shown in Fig. 5. Two parallel DHS networks served the high-rise and low-rise residential units separately. Units on and above 8th floors in high-rise towers were connected to a high-pressure secondary network. A low-pressure secondary network served the 6-storey slab buildings and the lower floors (below the 8th floor) of the high-rise towers. Both secondary networks derived heat inputs from the primary network via a heat exchanger situated at the basement between building D5 and D6. Information on the pipe fitting types, length, diameters, insulation attributes, and plan layout of the secondary networks were obtained from a collaborating heating supply company.

2.2.2. Measurement

Measurement of DHS network parameters and building indoor conditions were conducted at the CUT community between

Fig. 4. Site location and layout of the Central University Town residential community in Shenyang, China.

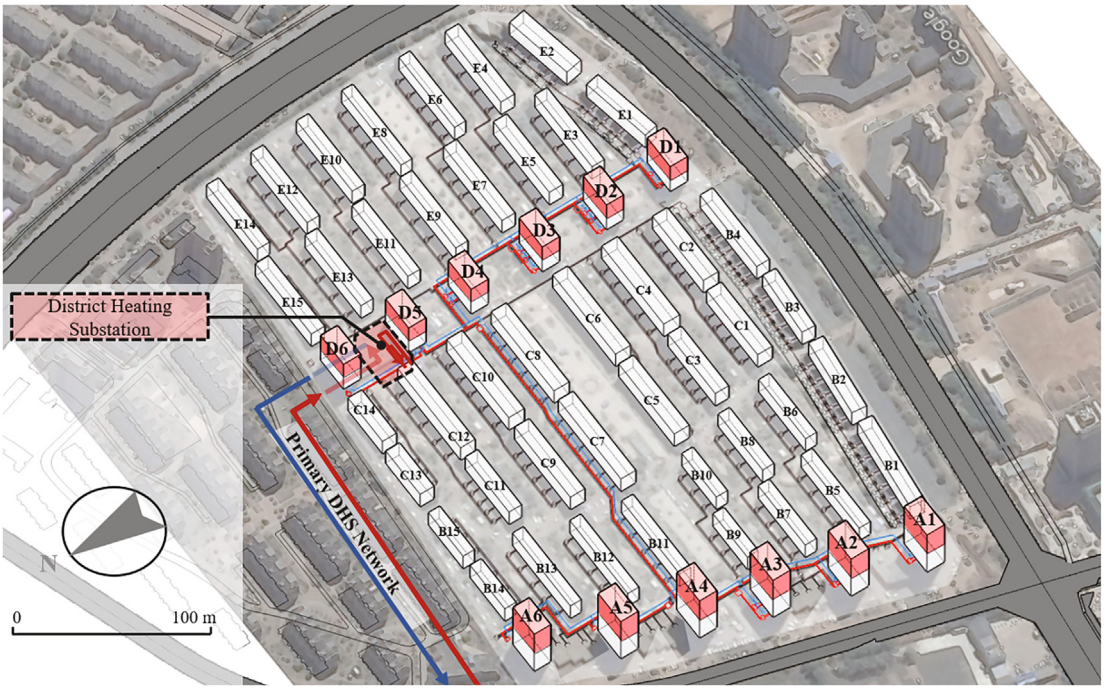

Fig. 5. An isometric view of the Central University Town residential community consisted of a district heating substation connected to the primary DHS network, 44 low-rise buildings, 12 high-rise towers (12–18 storey). The secondary DHS network, highlighted in red (supply) and blue (return), serves the higher floors (7 and above) of building A1-6 and D1-6. (For interpretation of the references to color in this figure legend, the reader is referred to the web version of this article.)

March1-16, 2017. The list of instruments and variables measured are summarized in Table 1 below.

The outdoor weather conditions were measured using a HOBO weather station mounted at the rooftop of the substation (Fig. 6 (a)). Air temperature, humidity, wind speed, and solar radiation were recorded at 5-min intervals and used as inputs for the simulation model described in Section 2.1.3.

Water temperature at the substation and buildings were measured from the pipeline surfaces using thermocouples (Center309) and recorded on a data logger (Agilent 34972A). The measurement

Table 1
Parameters recorded during field measurement in Central University Town, Shenyang.

Instrument Type	Quantity	Variables	Specification Range	Labelled Accuracy
Onset Temperature & RH Sensor (U23 Pro V2)	1	Outdoor Air Temperature	−40 to 70 °C	± 0.2 °C
		Outdoor Relative Humidity	0–100%	±2.5%
Onset Wind Speed & Direction Sensor (S-WCA-M003)	1	Outdoor Wind Direction	0–358°	±5.0°
		Outdoor Wind Speed	0–44 m/s	±0.5 m/s (<17 m/s) ±3% (17 to 30 m/s) ± 4% (30 to 44 m/s)
Onset Radiation Sensor (S-LIB-M003)	1	Global Horizontal Irradiance	0–1280 W/m^2	±10 W/m^2 or ± 5%
iButton (DS1922L)	20	Indoor Air Temperature	−40 to 85 °C	±0.5 °C
Thermocouple (Center309) Agilent34972A Data Acquisition Unit	6	Water temperature	0–100 °C	±1.0 °C
Ultasonic Flow Meter (Dalian Sonic FV4018)		Pipe water flow rate	−32 to 32 m/s	±1.0%

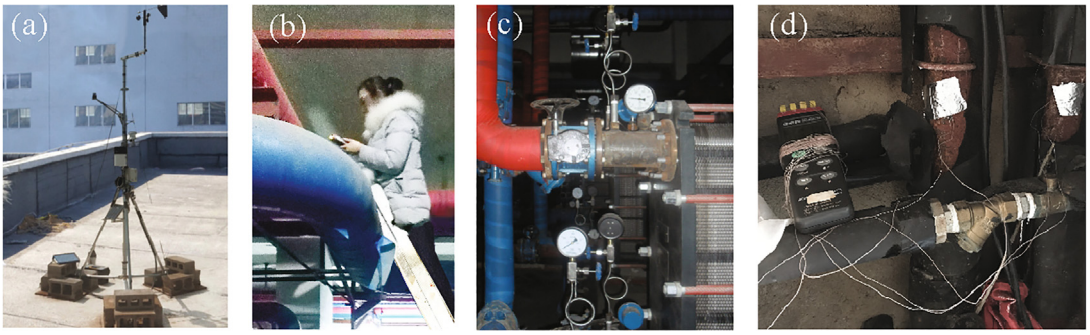

Fig. 6. a) Measurement of weather data from a rooftop HOBO weather station; b) Measurement of the water temperature at supply and return outlet in the substation; c) Measurement of the water flowrate and pressure head readings from the substation; d) Measurement of supply and return water temperature in the service duct of building blocks.

locations were at the heat exchanger (Fig. 6(b)) and the service duct of building A1 and A6 at both the supply and return pipes. As it is shown in Fig. 6(d), thermocouples were taped firmly to the steel pipe surface after cutting off the Polyurethane foam insulation layer and scratching off paint and metal rust from the surface. The flowrate of hot water out of the heat exchanger was measured using an ultrasonic flowmeter (Dalian Sonic FV4018) (Fig. 6(c)).

Indoor air temperatures inside residential units were measured using iButton (DS1922L). Measurements were conducted in 20 residential units from 13 buildings (A1, A6, C5, C1, C7, C11, D4, D6, E1, E4, E8 & E12) on a voluntary enrolment basis. The iButtons were placed in the living rooms of enrolled households for a period of 15 days, away from domestic heat sources and from direct sunlight. Air temperature data were recorded at 1 min interval. Two residential units enrolled in this study unsubscribed heating services from the DHS while remaining occupied during the study period.

2.2.3. Operational data

The operational data on the secondary DHS network of 51 residential communities, including the CUT community, were obtained during the heating season between Nov. 1, 2016 to 31 March 2017, covering a total of 8 million square meters of building floor space. The dataset consisted the supply and return water temperature, flow rate by design, electricity consumption at the circulator pump, and the metered water top-up rate as an indicator of water leakage.

2.3. Simulation setup

Simulations were conducted for the secondary DHS network serving the upper proportions of the CUT community. A schematic depiction is shown in Fig. 7. The secondary DHS network consisted of 43 nodes, each assumed to be homogeneous in internal pressure and temperature at each time step. The upper proportions (on and above 8th floor) of the 12 high-rise towers (A1-6, D1-6) were

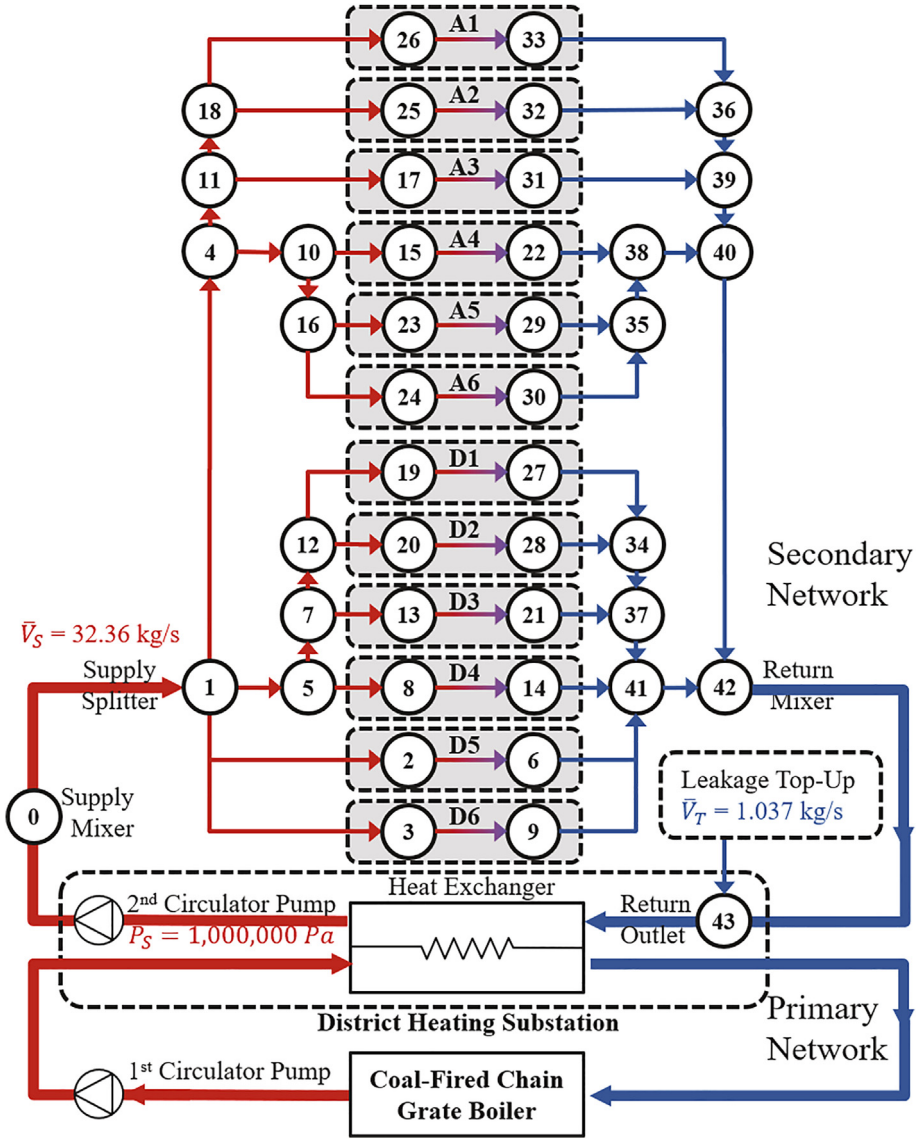

Fig. 7. A schematic depiction of the primary and secondary DHS network. The secondary network consists of a district heating substation, 44 nodes (0–43), the upper floors of the 12 building blocks (A1-6, D1-6), and a pipeline network of 2,788 m in length.

connected to the network, each tower was assumed to be linked to a supply and a return node, with the pipeline sections in-between treated as the radiant floor emitters transferring heat to indoor spaces. The heat exchanger was connected to the primary DHS network as the heat source, while a water leakage top-up tank was connected to the return outlet, which automatically compensated for water losses; leakage was found to be common according to the operational dataset mentioned in Section 2.2.3.

Parameters of the secondary DHS network, such as pipeline diameters, depth and insulation layers, were obtained from field survey The dimension parameters of the three types of steel pipes used in the study site is summarized in Table 2. The insulation layer was made of Polyurethane foam, with a standard thermal conductivity k_i of 0.03 W/m^{2}K. The pipeline network was buried at 1.6 m below ground. The monthly soil temperature in March at the depth of 1.6 m was estimated at −3.37℃ for Shenyang, according to EPW weather file from USDOE [48]. The pressure head at the supply mixer provided by the circulator pump (P_S) was taken from the standard labelled output at 1,000,000 Pa. The water flowrate (V_S) measured by the ultrasonic flow meter during the study period was between 28.61 and 36.11 kg/s, with the mean value at 32.36 kg/s.

Building energy use was modelled at the residential unit level for block A1 and A6, two high-rise towers located at the southwest and northwest corners of CUT. The aim was to compare simulated indoor air temperature with the measured data. Block A1 and A6 are the only two buildings connected to the secondary DHS network with concurrent temperature measurements of the indoor air temperatures, water temperatures at the supply and return of both buildings and the heat exchangers during the field studies, allowing for a detailed comparison between the measurement and simulation results.

A schematic depiction of the building blocks simulated is provided in Fig. 8. The upper floors of A1 and A6 (8 to 18 floor) were connected to the DHS pipeline. Each floor contained 10 residential units of various sizes and orientation, served by two elevators, a staircase, and a service duct. Each residential unit was modelled as a space in HTB2, with hot water flowrate assigned to each in proportion to the floor area of each unit. The elevators, staircase, and the service duct on each floor were modelled as unheated spaces. Building geometries, floor plan, façade and glazing were modelled based on construction drawings and photographic surveys. Shading from nearby buildings were unaccounted for in the simulation since both A1 and A6 have unobstructed solar access.

A radiant floor heating system was modelled in each residential unit according to surveyed construction details (Fig. 9). The hydronic tubing inside the floor measured 0.012 m in diameter, 200 m in total equivalent length per unit. The hourly supply water temperature was provided by simulated results from 2.1.1 and 2.1.2. The window-to-wall ratio, the G-value for window, U-values, and Air Changes Per Hour (ACPH) used in the simulation model were specified in Table 3, in reference to the Liaoning Province Energy Efficiency Design Standards for Residential Buildings [50]. The internal heat gains from electric equipment, lighting and occupancy input in the simulation model are summarized in Table 4, in reference to a combination of empirical studies of occupancy schedule in residential buildings in Northern China [51], the local code on building lighting design [52] and adjusted for the local lifestyle according to field surveys. To account for the thermal massing effect, the HTB2 model was run for a period of one week prior to actual simulation time.

3. Results and discussion

Model results were evaluated by comparing with field measurement data; Sensitivity analysis were performed to assess the effectiveness of retrofitting strategies.

Table 2
A list of steel pipe in the secondary DHS network by type and dimension (unit: m).

Pipe type [49]	DN250	DN125	DN100	DN80	DN25
Outer Radius (r_2)	0.1337	0.0699	0.0572	0.0446	0.0170
Inner Radius (r_1)	0.1271	0.0654	0.0527	0.0404	0.0138
Wall Thickness ($r_2 - r_1$)	0.0066	0.0045	0.0045	0.0042	0.0032
Thickness of Insulation (r_3-r_2)	0.0500	0.0500	0.0400	0.0400	0.0350

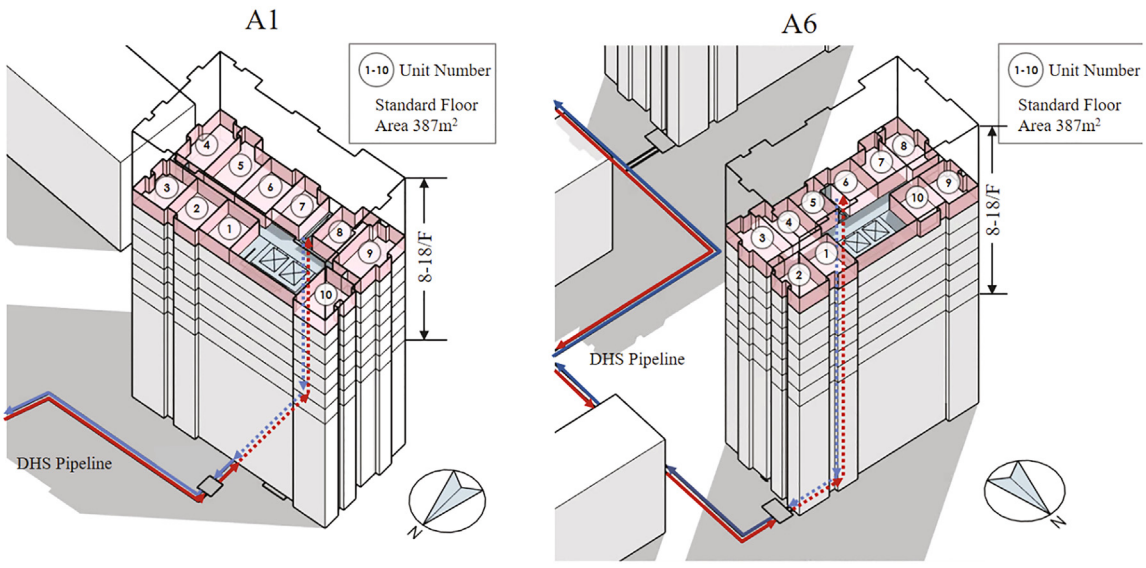

Fig. 8. Simulation schemes for the upper floors (8-18F) of the high-rise Block A1(left) and A6 (right).

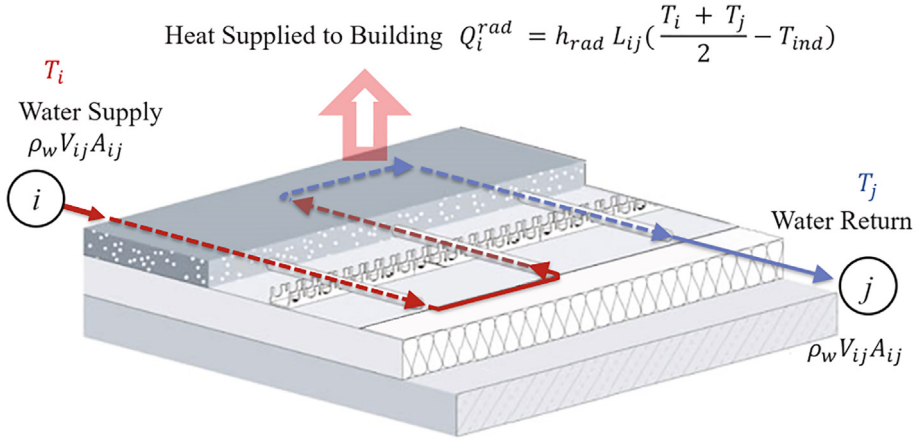

Fig. 9. Construction details of the radiant floor emitter inside building blocks.

Table 3
Building thermal properties and infiltration rate used in simulation.

Parameter	Window-to-Wall Ratio		Solar Factor (G-value)	U-Value (W/m^{2}K)					ACPH (times/hour)
	North Facade	Other Facades	Window	Roof	Exterior Wall	Exterior Door	Exterior Window	Ground	Residential Unit
Value	0.20	0.30	0.64	0.40	0.50	1.50	2.50	0.35	0.50

Table 4
Occupancy and small power schedule used in building simulation.

Time	Lighting (W/m^2)	Electric equipment (W/m^2)	Occupancy (ppl/unit)
0:00–5:00	1.4	1.0	3.0
6:00–8:00	5.6	4.0	3.0
9:00–10:00	0.7	0.5	0.3
11:00–13:00	0.0	0.0	0.0
14:00–16:00	0.7	0.0	0.3
17:00–18:00	3.5	0.5	1.5
19:00–22:00	5.6	2.5	2.4
23:00–0:00	1.4	4.0	3.0

3.1. Measurement data

The weather conditions during the study period of 1–16 March 2017 were sunny or cloudy, without precipitation nor snow cover on the ground. Data recorded at the HOBO weather station are summarized in Table 5.

The average flowrate out of the supply mixer of the secondary DHS network was 116.7 m^3/hr during the study period (ranging between 103.1 and 130.2 m^3/hr). The mean water flow speed from the water supply pipe (DN250) was measured at 0.71 m/s. Water top-up rate was measured at 89.6 tons of water per day during the heating season between 1 November 2016 to 31 March 2017. The average leakage rate was measured at 1.037 kg/s, which was 3.2% of the water flow within the secondary DHS network.

Table 5
Summary of onsite weather conditions during the field study in Shenyang 1–16 March 2017.

Parameters	Mean	Maximum	Minimum
Outdoor air temperature (℃)	−1.5	7.4	−9.5
Relative Humidity (%)	50.2	70.6	32.1
Wind Speed (m/s)	0.9	4.0	0.0
Global Solar Radiation (W/m^2)	178.9	706.9	0.0

Indoor air temperature measurement data revealed significant variations among the households enrolled in the studies (Fig. 10). Among the 18 households subscribing to heating services, the peak indoor air temperature recorded was 28.5 °C, while the lowest was at 14.0 °C. The mean indoor air temperature for the sample of 18 households stayed around 21.0 ± 1.0 °C, with the temperature gap between the hottest and coldest some 7.0 °C on average. The gap suggested that some households likely experienced heat stress while others were in cold stress: were there indoor thermostats or adjustment valves in the secondary DHS network, the thermal comfort and system energy efficiency could be improved. The measured air temperatures of the two free-rider units, which were disconnected from the DHS, were significantly lower than others, especially at night.

3.2. Model evaluation

Evaluation studies were conducted for blocks A1 and A6, two 18-storey high-rise residential buildings located at the western end of the secondary pipeline network (Fig. 5). Both blocks received unobstructed solar access, with no shading from surrounding buildings. Predicted supply, return water temperature and indoor air temperatures for each residential unit within the building were carried out for a period of 26 h between 11:00 March 5 and 13:00 March 6, 2017, in which measurements were conducted.

3.2.1. Measured and calculated water temperature

A reasonably good agreement was observed between measured and calculated water temperature both at the A1 building supply and return (Fig. 11). The scatter plot of predicted and measured water temperatures shows good agreement between the two for both the supply (R^2 = 0.66 and RMSE = 0.27 °C) and return (R^2 = 0.79, RMSE = 0.19), as it is shown in Fig. 12. Fig. 13 show the distribution of differences between predicted and measured water temperature; the BETHS model over-predicted the supply water temperature by 0.074 °C and under-predicted the return water temperature by 0.062 °C.

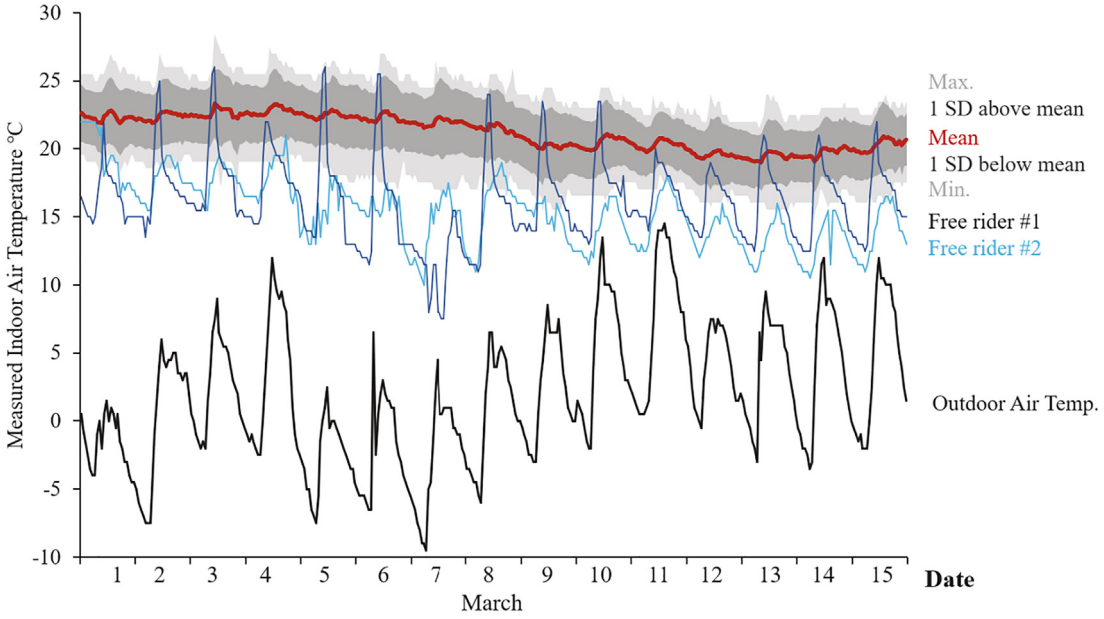

Fig. 10. Indoor air temperature measured in the living rooms of 18 residential units in 1–15 March 2017.

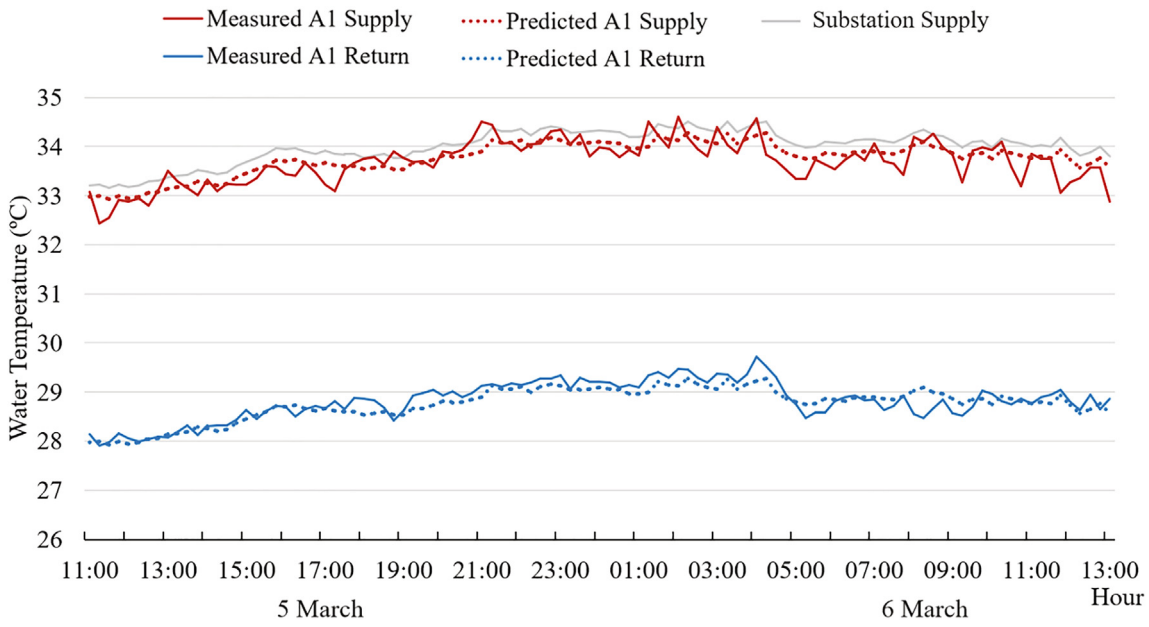

Fig. 11. Predicted and measured supply water temperature at block A1 in 5–6 March 2017.

3.2.2. Predicted building indoor air temperature

Predicted indoor air temperature followed closely the trend of the measurement data for the 5 residential units in blocks A1 and A6 (Figs. 14 and 15). A good agreement between measured and predicted indoor air temperatures were observed for Block A1. Due to solar heat gains, the indoor temperature for south-facing residential units 5, 6, 7 appears to be consistently higher than those of the north facing ones, as confirmed by both predicted and measurement data.

Predicted indoor air temperatures was reasonably close to the measurement data for Block A6. In Unit 6, there were periods when the measured indoor air temperature dropped significantly below the predicted level, after the indoor air temperature exceeded 26 °C, for instance, 18:00–23:00 on 17 March. It was likely that the occupants opened windows to reduce overheating. For Unit 2, the free-rider with unsubscribed heating services, it was plausible that the occupants used a space heater in replacement of the district heating. Measured temperature in Unit 2 started to rise at 7:00 in the morning, peaked at 10:00, and steadily dropped after 16:00 except for on 7 March when the space heater was disused, and the measured air temperature stayed below predicted level.

3.3. Sensitivity analysis

A sensitivity analysis was conducted in order to estimate the effectiveness of various energy savings strategies based on the main characteristics of the type DHS systems studied. Four simulation scenarios were carried out, including 1) the prevention of water leakage, a commonly found feature in our field studies, 2) reducing indoor air temperature, a behavioural adaptation

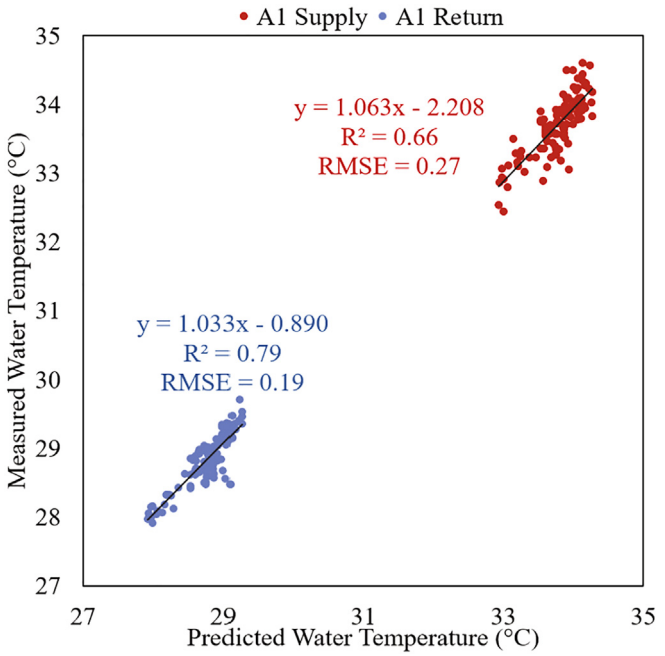

Fig. 12. A scatter plot of predicted and measured supply water temperature at block A1 in 5–6 March 2017.

requiring consensus; 3) improving building insulation, an energy-saving initiative actively pursued by the government, and 4) switching from coal to gas, a policy of growing importance in recent years [4] in an effort to seek alternative heat sources. Predicted energy savings potentials and GHG emissions for each scenario were calculated and compared. Implications were discussed relating to system maintenance, retrofitting and occupant behaviours.

3.3.1. Preventing water leakage

Water leakage mitigation was expected to save energy by reducing the need to heat the top-up water, assumed to be 4 °C out of the water main in Shenyang's winter, to the water supply temperature of some 34 °C. Predicted energy demand for the secondary DHS network as a function of water leakage rate is plotted in Fig. 16 below. The water leakage rate correlated positively with energy demand: every 1% increase in leakage rate was associated with 43.9kWh per hour increase in energy use. The existing secondary DHS network had a measured leakage rate of 3.2% and predicted energy demand of 823kWh per hour; a leakage-free system would therefore achieve an energy savings of 126kWh per hour, or 15.3% of the total energy demand compared with the existing condition.

3.3.2. Reducing indoor air temperature

The energy saving potential associated with a lower indoor air temperature were calculated for three presumptive scenarios in which the mean indoor air temperatures ($\overline{T}_{ind}$) were lowered to 19.5 °C, 17.9 °C and 16.4 °C from 21.2 °C of the existing condition. These assumptive scenarios were made in reference to the Adaptive Comfort Standard in ASHRAE Standard 55 [53], in which an Operative Temperature (OT) of 19.5 °C is close to the comfort temperature; while 17.9 °C and 16.4 °C are within the 90% and 80% acceptable range respectively (Fig. 17). Recognizing the ASHRAE Adaptive Comfort were measured in OT, we approximated OT to the indoor air temperature, a practical assumption often used in indoor thermal comfort studies where occupants engaged in near sedentary physical activities, not in direct sunlight, and air speeds were low (<0.1 m/s) [53]. The current mean indoor air temperature of 21.2 °C measured above the comfort temperature at 19.5 °C, suggesting potentials to reduce indoor air temperature and save energy.

Fig. 18 summarizes the predicted average hourly energy demand of the secondary DHS network under the above scenarios. In sum, a reduction of 1 °C in $\overline{T}_{ind}$ correlates with a reduction in energy demand of some 50 kWh per hour, or 6.1% of those of the existing condition. Although, for $\overline{T}_{ind}$ lower than 16.9 °C, the 90% acceptable threshold under the ASHRAE Adaptive Comfort Standard[53], the settings of indoor air temperature are essentially a trade-off between occupant thermal comfort and energy use.

3.3.3. Improving building insulation

The energy demand of the DHS under various building insulation options for the building envelope, i.e. walls, ceiling, roof, floors, windows and doors, were simulated. The insulation options were in reference to a number of current and historical building regulations in China and the UK in recent decades, such as the 1) UK Building Regulations 1995 Edition [54], 2) 2007 Liaoning Province Design Standard for Energy Efficiency of Residential Buildings [50], the standard at the time of the construction of the Central University Town, 3) UK Building Regulations 2010 Edition [55], and 4) Building Regulations 2016 Edition [56], the current UK standard for new dwelling buildings. The UK standards were referred to because it has evolved continuously over the last five

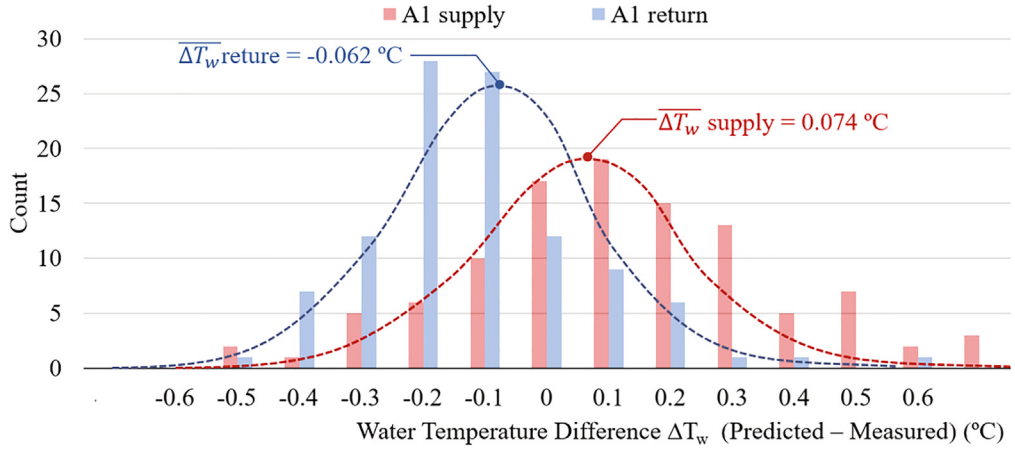

Fig. 13. Distribution of differences between predicted and measured water temperature at block A1 in 5–6 March 2017.

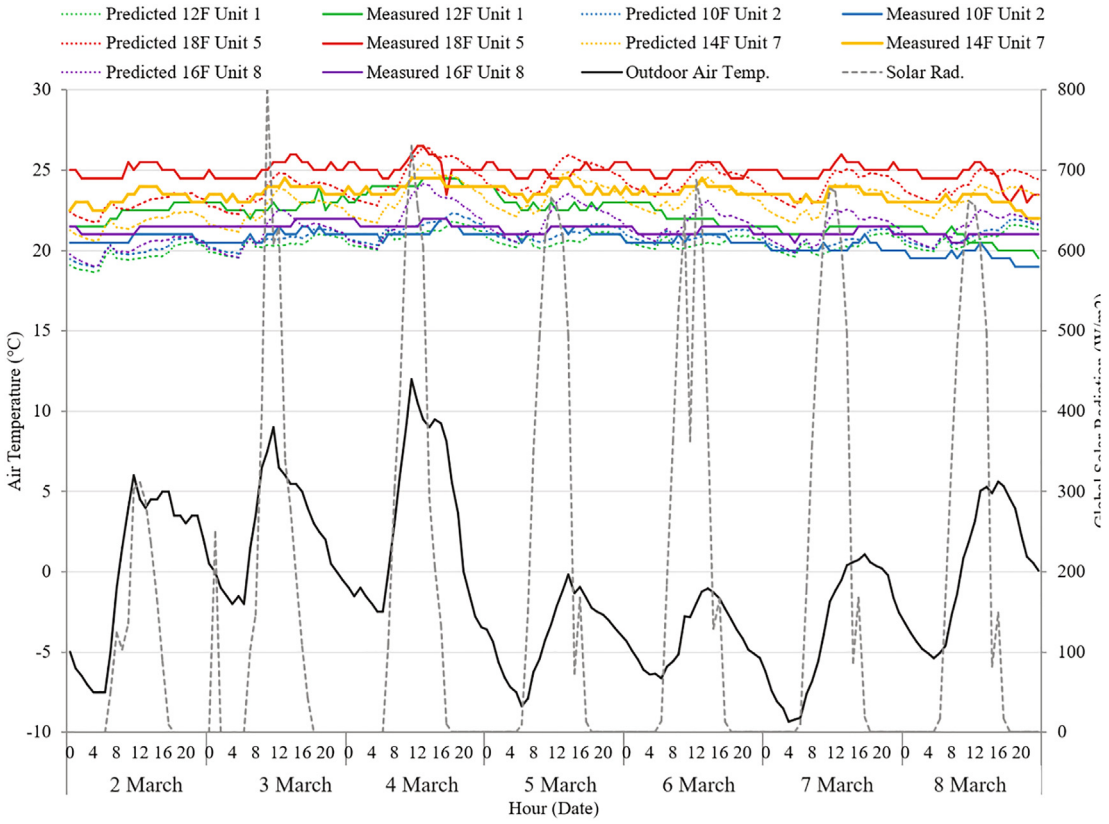

Fig. 14. Measured and predicted hourly indoor air temperature for residential units in building A1 in 2–8 March 2017.

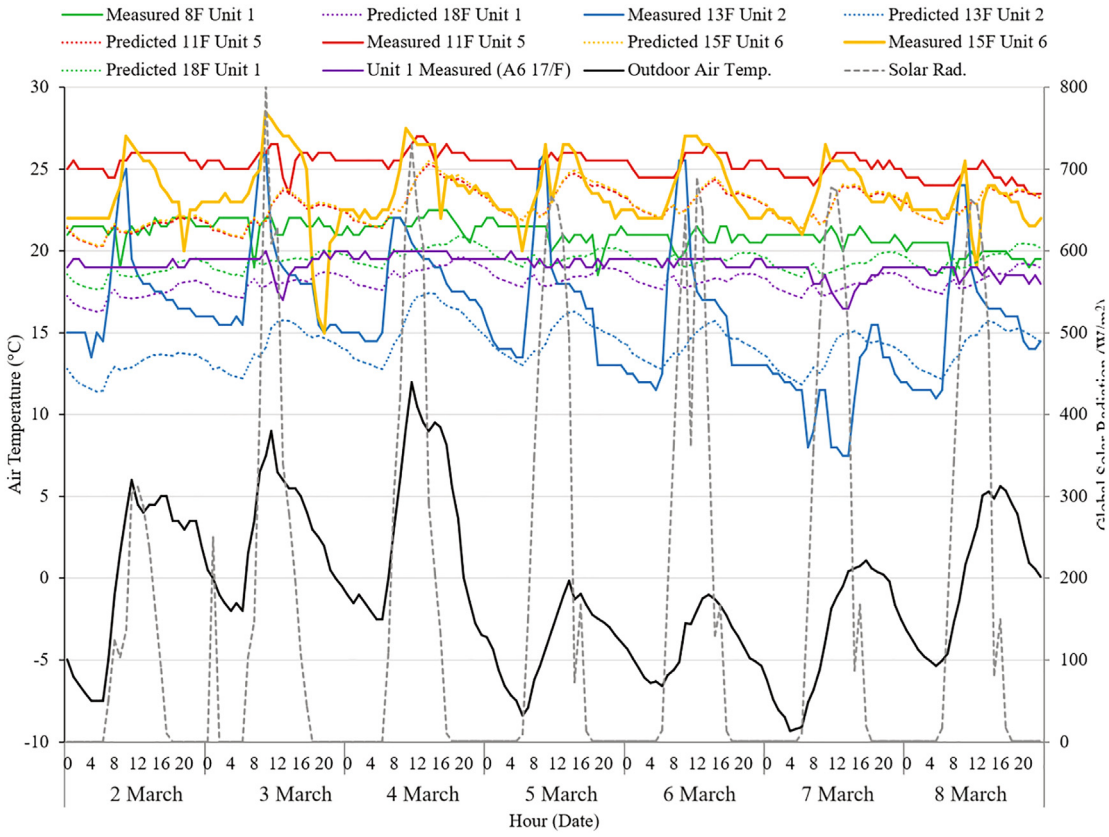

Fig. 15. Measured and predicted hourly indoor air temperature for residential units in Block A6 in 2–8 March 2017.

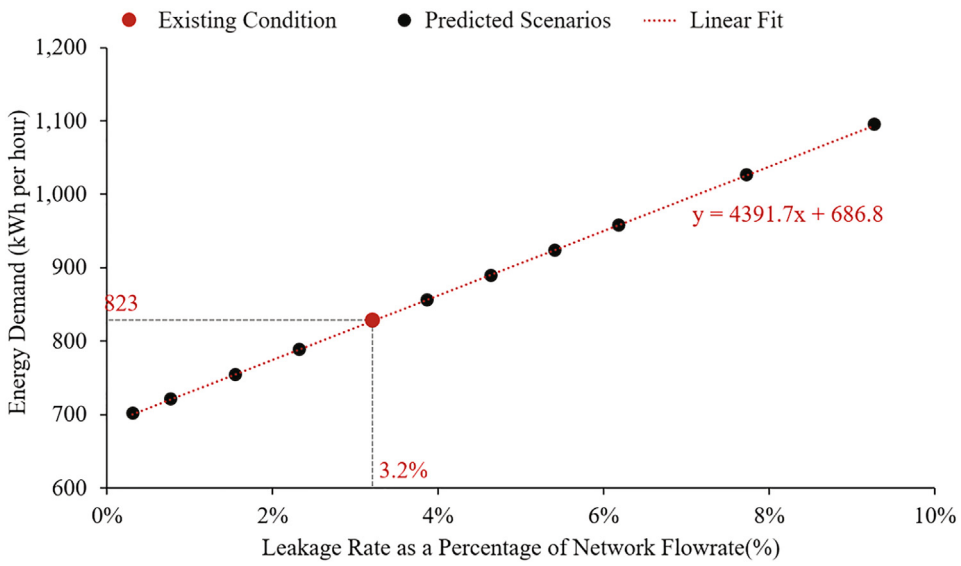

Fig. 16. Predicted averagely hourly energy demand for the secondary DHS network under a variety of pipe leakage conditions in 2–8 March 2017.

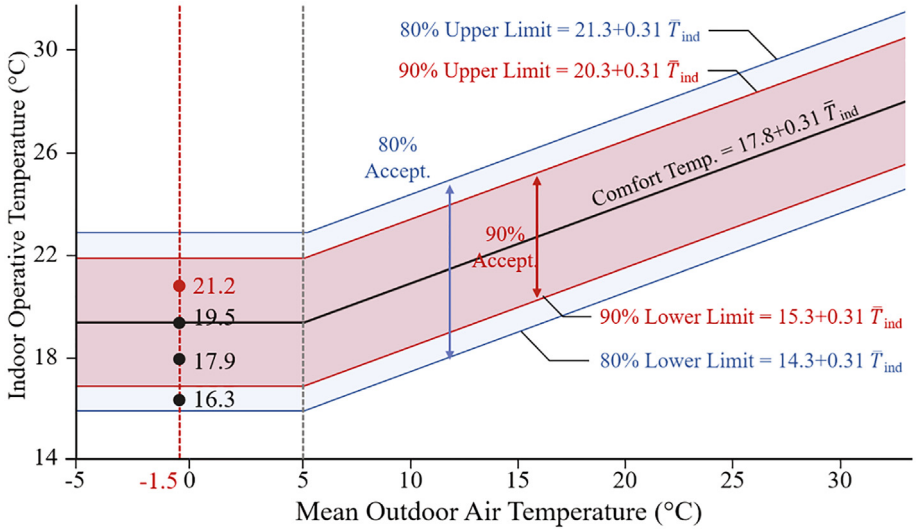

Fig. 17. Existing mean indoor temperature and three other scenarios used in this study plotted on top of the ASHRAE adaptive comfort standard [53]

decades to meet the homeowners' demand of reducing heating bills and increasing comfort.

Table 6 summarizes the simulation scenarios of the worst acceptable standards for building fabric properties. Multiple simulations were conducted in each scenario in order to plot the correlation between system energy demand and mean indoor air temperature $\overline{T}_{ind}$. Results are plotted in Fig. 19. Holding other attributes constant, the UK1991 is the most energy-intense of the four scenarios, while the UK2010 is the least energy-intense one. In order to maintain the same $\overline{T}_{ind}$ at 21.2 °C, an energy demand of 899kWh per hour is expected for the secondary DHS network under UK1995 scenario, 823kWh under LN2006, 672kWh under UK2010, and 523kWh under UK 2016. If the building insulation for the current study site can be upgraded from LN2007 to UK2016, an energy saving of 300kWh per hour is expected, which is equivalent to 31.5GWh per heating season or 36.5% of those under the existing condition.

3.3.4. Switching from coal to gas

The energy savings potential of converting the current coal-fired boilers with natural gas-fired ones have been calculated using simulated and labelled data. Coal-burning chain grate boilers were used during existing heating operations, which operate at a relatively low thermal efficiency of 60% according to literature [57]. A natural gas-fired boiler with heat recovery, in comparison, can achieve a thermal efficiency of 90% [58].

Figs. 20 and 21 shows the energy flow and system efficiency under coal-fired boilers and gas-fired boilers. Calculations were performed for the whole DHS network consisted of both the primary and secondary network. The system efficiencyη measures the thermal energy delivered to buildings as a percentage of the total energy input. Using coal-fired boilers, the total energy demand per heating season is 173.7 GWh; the system efficiency is 39.6%. In comparison, the total energy demand per heating season using natural gas-fired boilers is 118.8 GWh with a system

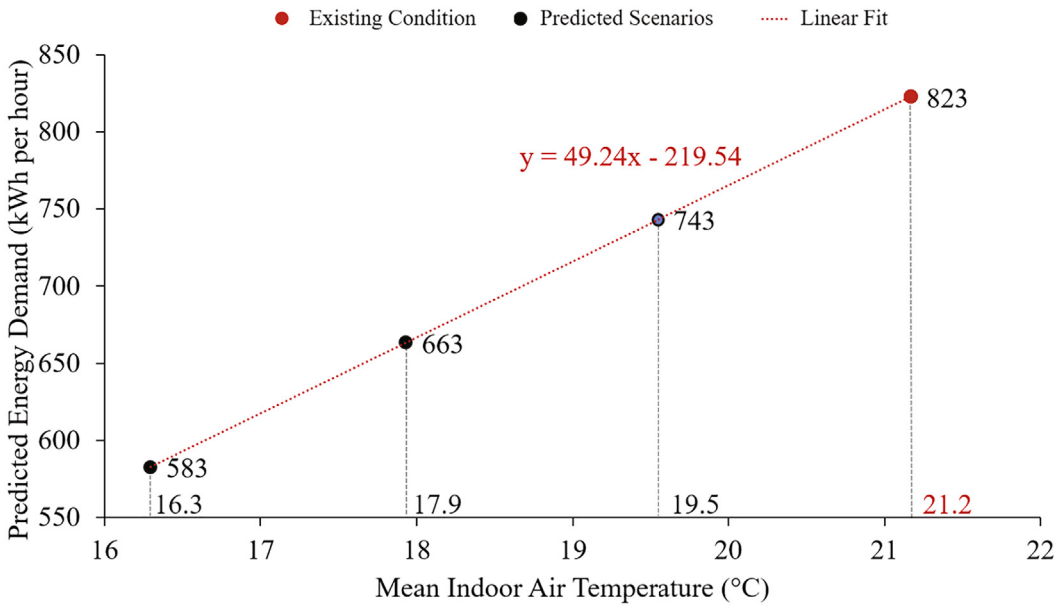

Fig. 18. Predicted average hourly energy demand for the secondary DHS network under a variety of indoor air temperature conditions in 2–8 March 2017.

Table 6
Summary of building insulation senarios as simulation inputs. Unit (W/m^2K).

Scenarios	UK1995 [54]	LN2006 [50]	UK2010 [55]	UK2016 [56]
Exterior Wall	0.45	0.5	0.3	0.18
Ceiling (Roof)	0.35	0.4	0.2	0.13
Floor	0.51	0.35	0.25	0.13
Window	3.0	2.5	2.0	1.4
Door	3.0	1.5	2.0	1.0

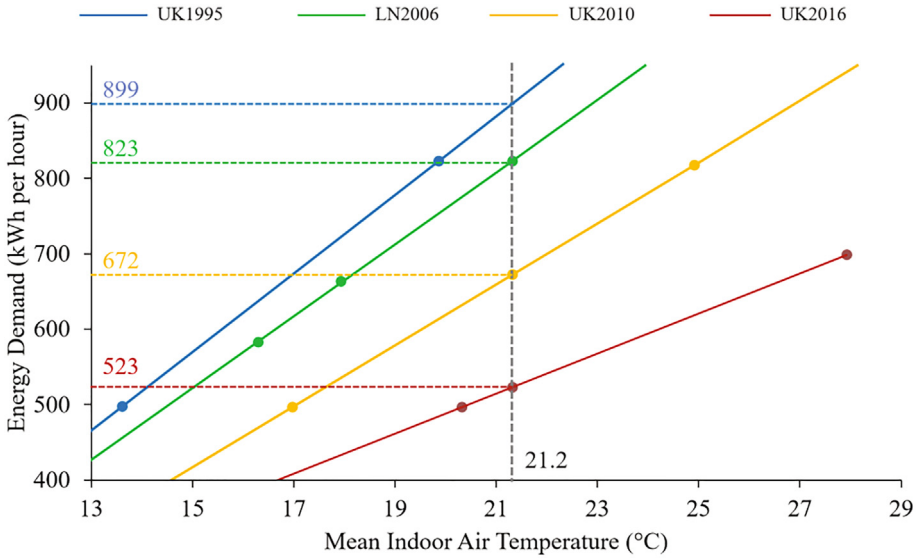

Fig. 19. Predicted average hourly energy demand for the secondary DHS network under a variety of building insulation and indoor air temperatures in 2–8 March 2017.

efficiency at 58.0%. By switching from coal to gas, an energy saving of 54.9 GWh is expected per heating season. A limitation for this estimate is that the primary DHS network has not been measured in field studies. Instead, the performances were inferred based on equipment label data collected from the field surveys. The solid color shows simulated and measured data. The hatched color shows best estimates from labelled data.

For the secondary DHS network, the total energy input measured at 86.4 GWh per heating season; the majority (83.9 GWh) were from the heat exchanger and a small fraction of 2.5 GWh were from the secondary circulator pump. 68.8 GWh of heating service was delivered to buildings, while 13.5 GWh and 4.1 GWh of energy were lost to water leakage and conductive heat loss along DHS pipeline respectively. For the secondary DHS network alone,

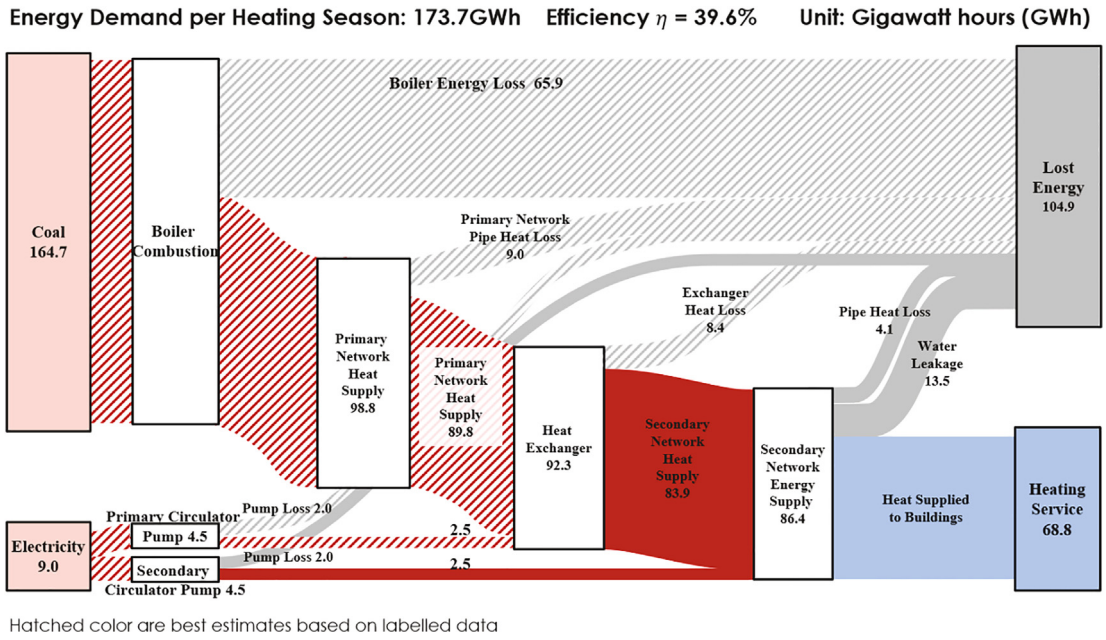

Fig. 20. Predicted DHS energy demand and system efficiency using coal-fired chain grate boilers.

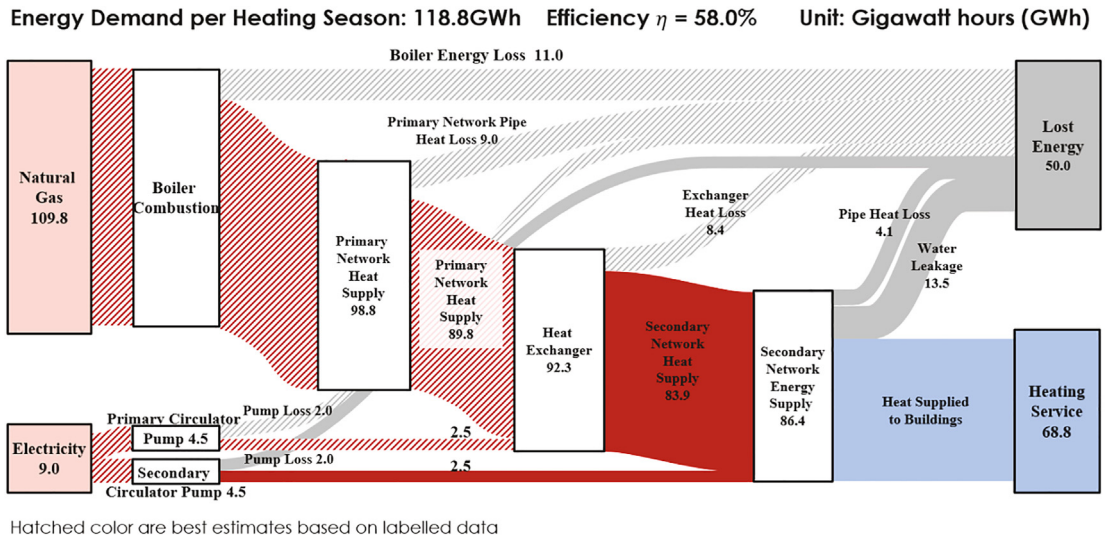

Fig. 21. Predicted DHS energy demand and system efficiency using natural gas-fired boilers with heat recovery.

the system efficiency equals 79.6%, which stood below the 90% required by the local standard [50].

3.4. Discussion

The coupled simulation model BETH can account for the hourly feedback between the DHS pipelines and buildings; therefore, it enables a dynamic estimate of the system performance over time. The coupled simulation can predict the hourly fluctuation of indoor air temperature of overheating or underheating (Figs. 14 and 15), which can reveal the inadequacies of the existing system and inform design, operation, and retrofitting decisions. The coupled model can also be used to calculate the return water temperature from building and back to the heat exchanger, allowing for a dynamic estimate of the heating load at the heat exchanger and the system efficiency. A decoupled model, in the absence of the feedback, usually relies on simplifications made either of an assumed indoor temperature profile, or an assumed rate of heating supply from the DHS pipeline. Both assumptions are expected to deviate from the real conditions.

The BETHS model can better support decision-making by comparing energy savings and GHG emission reductions across multiple operational, maintenance, and retrofitting options. Fig. 22 shows such a comparison under various energy saving strategies of 1) Leakage Prevention, 2) Indoor Air Temperature Reduction, 3) Switch from Coal to Gas, and 4) Building Retrofit by UK 2016 Standard. The GHG emission was calculated based on China's life-cycle GHG emission factors for coal (0.108 kgCO2, e/MJ) and gas (0.068 kgCO2, e/MJ) obtained from research literature [59].

Building energy retrofit, which is a one-off technical solution, demonstrated the largest energy saving potential among the four, and the second largest GHG emission reduction. By upgrade the building envelope of the upper floors of the 12 residential towers to the current UK building regulation standard, i.e. installation of

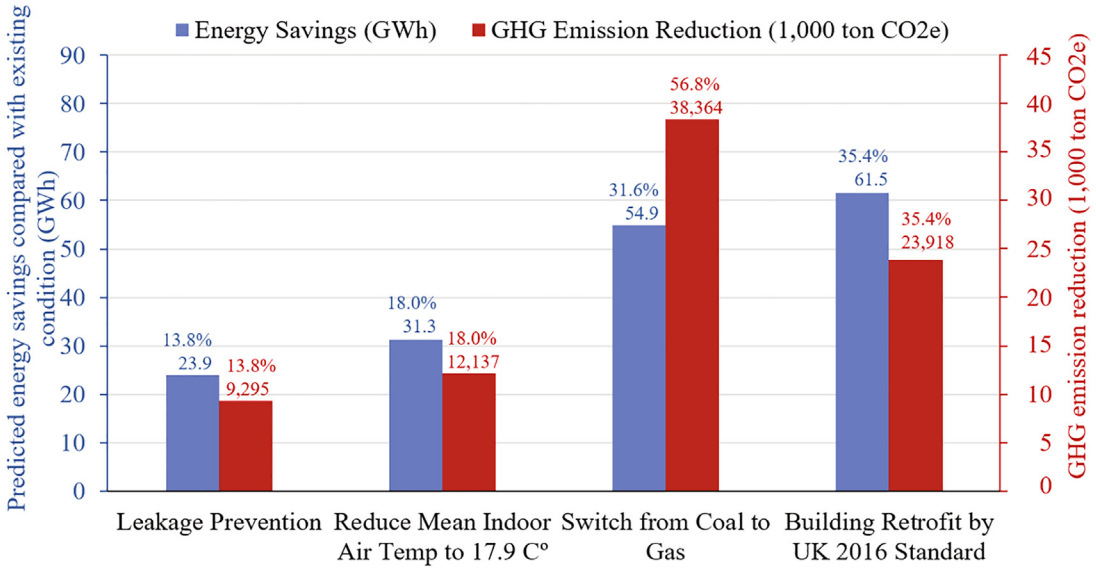

Fig. 22. Energy saving potentials and GHG emission reductions for the DHS of the Central University Town under 1) Leakage Prevention, 2) Indoor Air Temperature Reduction, 3) Switch from Coal to Gas, and 4) Building Retrofit by UK 2016 Standard as a percentage of energy demand under existing condition per heating season.

additional wall insulation, upgrade of windows and doors, an energy saving of 61.5GWh and a GHG emission reduction of 23,918 tons of CO2e is expected per heating season. This translates roughly into 35.4% of total energy savings from the DHS network and GHG emission reduction. For the 52 residential communities of 6.9 million square meters of building floor area, the energy saving potentials of the energy retrofit strategy is expected to be 101,500,000 GWh per heating season, or GHG emission reduction of over 39 million tons. Findings from this study support the current policy priority on building envelope insulation, developed by the Chinese National Development and Reform Commission in the "Northern Region Winter Clean Heating Planning 2017–2021" [4].

Converting existing coal-fired chain grate boiler to natural gas-fired boiler with heat recovery can achieve the largest GHG emission reduction and significant energy saving, measuring at 38,364 tons of CO2e and 54.9 GWh per heating season. For the 52 residential communities of 6.9 million square meters of building floor area, the GHG emission reduction is expected to be over 63 million tons in CO2e per heating season, and the energy saving potentials to be 90,600,000 GWh. The health benefits associated with switching from coal to gas in terms of reduced air pollutants is expected to be significant. However, switching from coal to gas requires a large investment upfront, and a high operational cost of a natural gas fired boiler because of the relatively high price of the fuel gas in China [60]. Despite significant GHG emission reduction and energy savings, it may not the most cost-effective option in the context of this study.

Reducing mean indoor air temperature, which requires a social commitment to accept a lower indoor air temperature, is expected to deliver considerable energy savings and GHG emission reduction. By reducing the mean indoor air temperature from the cur-

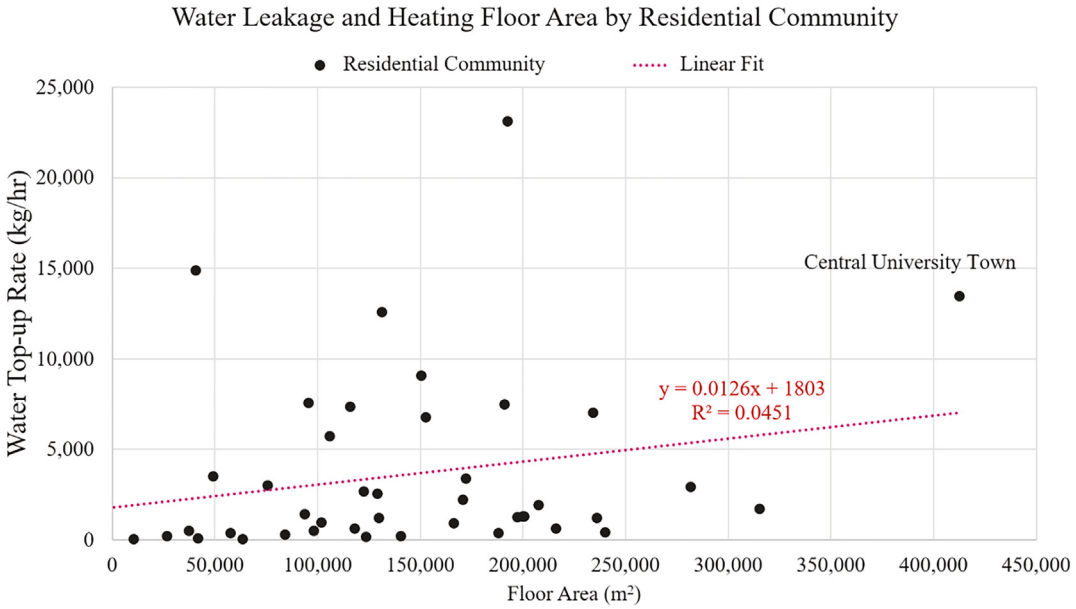

Fig. 23. Water Leakage and Heating Floor Area of 51 Residential Communities in Shenyang during the heat season between 1 November 2015 and 31 March 2016.

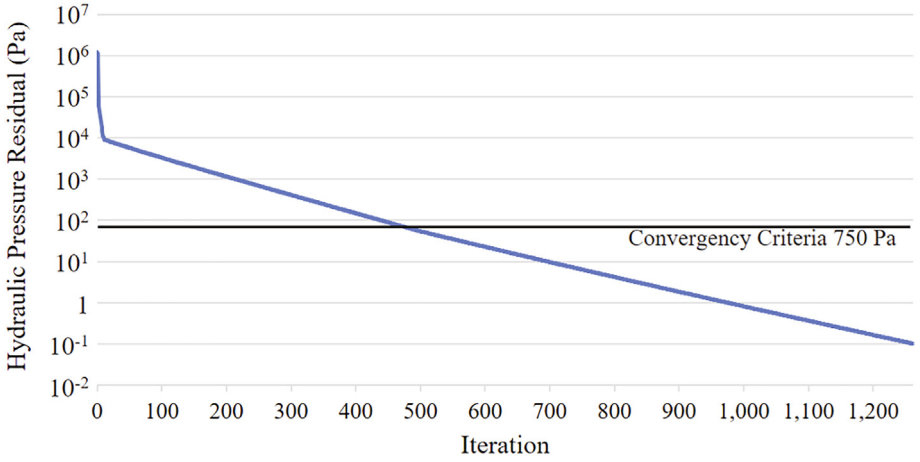

Fig. 24. The convergence performance for the BETHS thermo-hydraulic model.

rent 21.2 to 17.9 °C, an energy saving of approximately 31.3 GWh per heating season and a GHG emission reduction of 12,317 tons in CO2e for the secondary DHS network in Central University Town, or 51,700,000 GWh and over 20 million tons of CO2e for the 52 residential communities combined. A practical barrier to implementation of this strategy is the need for dynamic control of water flow and room temperature in order to overcome the uneven indoor air temperature distribution observed in field studies (Fig. 10). In the absence of a dynamic flow control mechanism and unit thermostat, which is a common challenge for the majority of DHS networks in Northern China [6], a heating supply company risks customer complaints over unsatisfactorily room temperatures, which leads to an economic disincentive for DHS operators to do so.

Lastly, water leakage prevention, as a component of routine maintenance, can deliver considerable energy savings. The presence of leakage in the high-rise secondary network of the Central University Town is the primary reason why the heating delivery efficiency of the secondary DHS network is below the 90% mandated by the local standard [42]. Water leakage is common according to our field survey in the 52 residential communities in Shenyang; water top-up rate dataset suggested a number of secondary DHS network suffered from a sizable leakage as it is shown in Fig. 23, in which the water top-up rate normalized for the duration of the heating season between 1 October 2015 and 31 March 2016 was plotted against the total floor area served by DHS. Leakage rate correlated positively with building floor area in a residential community. A linear fit line suggests that for each 1,000 m^2 of floor area added to DHS service, an additional water leakage of 12.6 kg/hr. is expected during the heating season. A back-of-the-envelope calculation based on the correlation established in Fig. 16 suggests if the water leakage rate can be reduced by half for the top 5 communities of the highest leakage rate, the potential energy savings will be 533.0GWh per heating season, or a reduction of 207,000 tons of CO2e. For existing systems with detectable leakage, inspections are needed to allow operators to localize and repair leakage segments. Proper maintenance is needed to prevent pipe erosion and degradation.

A combined energy saving of 117.0GWh per heating season, or 67% of those under the existing condition is expected if the four strategies, i.e. building energy retrofit, switching from coal to gas, reducing mean indoor air temperature, and water leakage prevention are adopted together. Once combined with practical constraints and costing data, the BETHS model can be used to predict the cost-effectiveness of energy saving strategies for existing DHS network and building stocks.

Computationally, the BETHS model ran efficiently with satisfactory convergence. The hydraulic pressure residual ΔP is plotted over iteration in Fig. 24. For the 12-building, 46-node DHS network on an ordinary laptop computer (CPU 2.11 GHz, RAM 32.0 GB), the model takes approximate 4 s for ΔP to converge under the pre-set threshold of 750 Pa, or 0.1% of the working pressure for the secondary DHS network which is the labelled accuracy for common water pressure sensors. Given the computational efficiency, the model enables hourly simulation for the heating season under dynamic water flow, weather and building operational conditions.

The next steps are to integrate BETHS model with the Virvil plugin developed at Cardiff University [24] to account for building mutual shadings. This is especially important in compact cities in which buildings shade each other and affect heating load interactively. heating service should account for solar heat gains and occupancy, which vary hourly depend on the massing, orientation, and lifestyle. Future application of the BETHS model include the support for design stage energy simulation mandated by the Chinese national design standards [61]. The BETHS model is to be applied to inform predictive operation of the DHS network. Instead of relying on personal experience, operators can adjust DHS water flow at the level of buildings and residential units, using simulated energy demand based on weather forecast and occupancy data. If successful, this method is expected to provide additional energy savings and improvement of occupant thermal comfort. The BETHS model also has potentials to model district cooling scenarios in hot climates.

4. Conclusion

This paper described a coupled thermo-hydraulic and building energy model, BETHS, developed to assess the time-varying energy performance and occupant thermal comfort for a cluster of buildings served by district heating systems in an urban context. The BETHS model was evaluated using measurement data collected from a residential community in Shenyang, China. Predicted water temperature of the DHS network and at residential unit level agreed reasonably well with measurement data. Sensitivity studies were conducted to identify energy savings potentials, in which water leakage prevention, reducing indoor air temperature, improving building insulation and switching from coal to natural gas were evaluated and compared with each other. Results showed the effectiveness of various energy saving strategies: improving building insulation to current UK standards can deliver 35% energy

savings from those of the existing condition, 32% for switching from coal to gas, 18% and 14%, respectively, for reducing indoor air temperature and leakage prevention. A combined energy saving of 67% was expected from all four strategies. The model demonstrated its potential use in supporting retrofit strategies and operational decisions for existing DHS systems. The strength of the BETHS model lies in its ability to account for the dynamic feedback between DHS pipelines and buildings. It is computationally efficiency, and compatibility with existing building energy simulation platforms. The next step is to integrate the BETHS model in building energy simulation software such as HTB2 to meet the practical need for such a module.

CRediT authorship contribution statement

Jianxiang Huang: Conceptualization, Methodology, Formal analysis, Writing - original draft. **Yi Xu:** Validation, Project administration, Visualization, Writing - original draft. **Phil Jones:** Conceptualization, Methodology, Investigation. **Xiaojun Li:** Software, Formal analysis. **Mengdi Guo:** Validation. **Gang Liu:** Supervision. **John S. Ji:** Resources.

Declaration of Competing Interest

The authors declare that they have no known competing financial interests or personal relationships that could have appeared to influence the work reported in this paper.

Acknowledgements

The research is partially supported by a grant from the National Science Foundation of China (51978594), a SEED grant from the Faculty of Architecture at the University of Hong Kong. The research benefited from the Distinguished Visiting Research Professorship from the Faculty of Architecture, University of Hong Kong (2015-17). We thank Prof. Yuguo Li of the University of Hong Kong for lending us the HOBO weather station, iButtons, and Thermocouples.

References

[1] ASHRAE, District Heating Guide. Atlanta, GA: American Society of Heating, Refrigerating and Air-Conditioning Engineers, Inc. (ASHRAE), 2013.
[2] A. Poredos, A. Kitanovski, District heating and cooling for efficient energy supply, *Proceedings* (2011) 5238–5241.
[3] S. Frederiksen, S. Werner, *District Heating and Cooling*, AB, Lund, Sweden: Studentlitteratur, 2013.
[4] NDRC, "Northern Region Winter Clean Heating Planning 2017-2021," 2017. [Online]. Available: http://www.ndrc.gov.cn/zcfb/zcfbtz/201712/t20171220_871052.html. [Accessed: 01-Mar-2020].
[5] IEA, "Tracking Clean Energy Progress," 2019. [Online]. Available: https://www.iea.org/tcep/.
[6] M. Gong, S. Werner, An assessment of district heating research in China, Renew. Energy 84 (2015) 97–105, https://doi.org/10.1016/j.renene.2015.05.061.
[7] MHURD, "Technical specification for energy efficiency retrofitting of existing residential buildings JGJ/T 129-2012," 2012.
[8] L. Xin, W. Chenchen, L. Chuanzhi, F. Guohui, Y. Zekai, L. Zonghan, Effect of the energy-saving retrofit on the existing residential buildings in the typical city in northern China, Energy Build. 177 (2018) 154–172, https://doi.org/10.1016/j.enbuild.2018.07.004.
[9] Euroheat and Power, "District Heating and Cooling country by country Survey 2015," 2015. [Online]. Available: http://www.euroheat.org/wp-content/uploads/2016/03/2015-Country-by-country-Statistics-Overview.pdf.
[10] DBDH, "Country by Country 2013 Survey: District Heating in Russia," 2013. [Online]. Available: https://dbdh.dk/download/member_contries/russia_and_sng/RUSSIA country by country.pdf.
[11] EIA, "U.S. District Energy Services Market Characterization," Washington DC, 2018. [Online]. Available: https://www.districtenergy.org/HigherLogic/System/DownloadDocumentFile.ashx?DocumentFileKey=44c35916-f1af-6bed-2fed-823299b36bde&forceDialog=0.
[12] S. Werner, International review of district heating and cooling, Energy 137 (2017) 617–631, https://doi.org/10.1016/j.energy.2017.04.045.
[13] H. Palsson, *Methods for planning and operating decentralized combined heat and power plants*. Kgs, Risø & DTU - Department of Energy Engineering (ET, Lyngby, Denmark, 2000.
[14] C. Arsene, A. Bargiela, D. Al-Dabass, Modelling and Simulation of Water Systems Based on Loop Equations, J. Simul. 5 (1) (2004) 1–2.
[15] A.G. Collins, R.L. Johnson, Finite-element method for water-distribution networks, J. Am. Water Works Assoc. 67 (7) (1975) 385–389.
[16] R. Donachie, Digital program for water network analysis, J. Hydraul. Div. 100 (3) (1974) 393–403.
[17] I. Hassine and U. Eicker, "Simulation and optimization of the district heating network in Scharnhauser Park," 2nd Eur. Conf. Polygeneration, vol. 49, no. 0, pp. 1–18, 2011.
[18] L. Liu, Y. Liu, W. Huang, C. Bao, Y. Zhao, Hydraulic regime analysis of on-off valve regulation, Appl. Mech. Mater. 522–524 (2014) 1009–1014.
[19] D. Knutsson, J. Sahlin, S. Werner, T. Ekvall, E.O. Ahlgren, HEATSPOT – A simulation tool for national district heating analyses, Energy 31 (2–3) (2006) 278–293, https://doi.org/10.1016/j.energy.2005.02.005.
[20] B. Talebi, P. A. Mirzaei, A. Bastani, and F. Haghighat, "A review of district heating systems: Modeling and optimization," Frontiers in Built Environment, vol. 2. 2016, doi: 10.3389/fbuil.2016.00022.
[21] P.T. Lewis, D.K. Alexander, HTB2: a flexible model for dynamic building simulation, Build. Environ. 25 (1) (Jan. 1990) 7–16, https://doi.org/10.1016/0360-1323(90)90035-P.
[22] D.B. Crawley, L.K. Lawrie, F.C. Winkelmann, W.F. Buhl, Y.J. Huang, C.O. Pedersen, R.K. Strand, R.J. Liesen, D.E. Fisher, M.J. Witte, J. Glazer, EnergyPlus: Creating a new-generation building energy simulation program, Energy Build. 33 (4) (2001) 319–331, https://doi.org/10.1016/S0378-7788(00)00114-6.
[23] W.A. Beckman, L. Broman, A. Fiksel, S.A. Klein, E. Lindberg, M. Schuler, J. Thornton, TRNSYS The most complete solar energy system modeling and simulation software, Renew. Energy 5 (1-4) (1994) 486–488, https://doi.org/10.1016/0960-1481(94)90420-0.
[24] P. Jones, S. Lannon, X. Li, T. Bassett, and D. Waldron, "Intensive Building Energy Simulation At Early Design Stage," in Proceedings of BS 2013: 13th Conference of the International Building Performance Simulation Association, 2013.
[25] R. Christoph F, D. Timur, J. J Alstan, R. Tarek, and S. Andrew, "Umi - an Urban Simulation Environment for Building Energy Use , Daylighting and Walkability," Proc. BS2013 13th Conf. Int. Build. Perform. Simul. Assoc., pp. 476–483, 2013.
[26] D. Robinson et al., "CITYSIM: Comprehensive Micro-Simulation Of Resource Flows For Sustainable Urban Planning," in International IBPSA Conference, 2009, pp. 1083–1090.
[27] M. Musy, E. Wurtz, F. Winkelmann, F. Allard, Generation of a zonal model to simulate natural convection in a room with a radiative/convective heater, Build. Environ. 36 (5) (2001) 589–596, https://doi.org/10.1016/S0360-1323(00)00043-3.
[28] R. Yao, Q. Luo, B. Li, A simplified mathematical model for urban microclimate simulation, Build. Environ. 46 (1) (Jan. 2011) 253–265, https://doi.org/10.1016/j.buildenv.2010.07.019.
[29] W. Liang, J. Huang, P. Jones, Q. Wang, J. Hang, A zonal model for assessing street canyon air temperature of high-density cities, Build. Environ. 132 (2018) 160–169, https://doi.org/10.1016/j.buildenv.2018.01.035.
[30] T. Hong, Y. Jiang, A new multizone model for the simulation of building thermal performance, Build. Environ. 32 (2) (1997) 123–128, https://doi.org/10.1016/S0360-1323(96)00045-5.
[31] Y. Li, A. Delsante, J. Symons, Prediction of natural ventilation in buildings with large openings, Build. Environ. 35 (3) (2000) 191–206, https://doi.org/10.1016/S0360-1323(99)00011-6.
[32] M.S. Al-Homoud, Computer-aided building energy analysis techniques, Build. Environ. 36 (4) (2001) 421–433, https://doi.org/10.1016/S0360-1323(00)00026-3.
[33] G.Y. Yun, K. Steemers, Behavioural, physical and socio-economic factors in household cooling energy consumption, Appl. Energy 88 (6) (2011) 2191–2200, https://doi.org/10.1016/j.apenergy.2011.01.010.
[34] E. Saloux, J.A. Candanedo, Forecasting District Heating Demand using Machine Learning Algorithms, Energy Procedia 149 (2018) 59–68.
[35] H.S. Hippert, C.E. Pedreira, R.C. Souza, Neural networks for short-term load forecasting: a review and evaluation, IEEE Trans. Power Syst. 16 (1) (2001) 44–55, https://doi.org/10.1109/59.910780.
[36] Y. Yamaguchi, Y. Shimoda, M. Mizuno, Development of district energy system simulation model based on detailed energy demand model, Proceeding Eighth Int. IBPSA Conf. (2003) 1443–1450.
[37] J. Ortiga, J. C. Bruno, A. Coronas, and I. E. Grossman, "Review of optimization models for the design of polygeneration systems in district heating and cooling networks," vol. 24, pp. 1121–1126, 2007, doi: 10.1016/S1570-7946(07)80211-2.
[38] B. Talebi, P.A. Mirzaei, A. Bastani, F. Haghighat, A review of district heating systems: modeling and optimization, Front. Built Environ. 2 (2016) 22.
[39] Esteban Estrella Guillen, Holly W. Samuelson, Christine Vohringer, The impact of cultural assumptions on simulated energy, comfort, and investment returns of design decisions in two desert climates, Build. Simul. 14 (4) (2021) 931–944, https://doi.org/10.1007/s12273-020-0718-y.
[40] ASHRAE, ASHRAE Handbook: Fundamentals, ASHRAE, Atlanta, GA, 2013, p. 2013.
[41] E.S. Menon, Transmission Pipeline Calculations and Simulations Manual, Gulf Professional Publishing, Houston, USA, 2015.

[42] Oscar Faber and Partners, "IEA Annex 1 Computer Modelling of Building Performance: Results and Analyses of Avonbank Simulation," St. Albans, UK, 1980.
[43] K. J. Lomas, H. Eppel, C. Martin, and D. Bloombield, "Empirical validation of detailed thermal programs using test room data, Volume 1: Final Report," 1994.
[44] J. Neymark, R. Judkoff, D. Alexander, P. Strachan, and A. Wijsman, "IEA BESTEST Multi-Zone Non-Airflow In-Depth Diagnostic Cases," 12th IBPSA, Sydney, no. November, pp. 14–16, 2011, [Online]. Available: http://www.nrel.gov/docs/fy12osti/51589.pdf.
[45] CMA, "Dataset of monthly surface observation values in individual years (1981-2010) in China," 2019. http://data.cma.cn/ (accessed Aug. 20, 2019).
[46] The Government of Shenyang, "The City of Shenyang Urban Heating Planning (2013-2020)," Shenyang, 2014.
[47] Heat China, "Urban heating development status and supply-demand analysis for Chinese Cities," The 15th China Heat Energy Exhibition, 2018. http://www.heat-china.com/article/show_article.php?id=972 (accessed Jul. 27, 2019).
[48] USDOE, "Weather Data for Simulation," 2020. https://energyplus.net/weather/sources (accessed Jun. 01, 2017).
[49] ISO, "ISO 6708:1995 Pipework Components - Definition and Selection of DN (Nominal Size)," 1995. iso.org/standard/21274.html (accessed Jun. 01, 2020).
[50] HCD, "Liaoning Province Design Standard for Energy Efficiency of Residential Buildings," Liaoning Province, China, 2006.
[51] S. Hu, D. Yan, J. AN, S. Guo, and M. Qian, "Investigation and analysis of Chinese residential building occupancy with large-scale questionnaire surveys," Energy Build., vol. 193, no. 15, pp. 289–304, 2019.
[52] AQSIQ, "GB50034-2004 Standard for lighting design of buildings," 2004. [Online]. Available: https://www.codeofchina.com/standard/GB50034-2004.html.
[53] G. S. Brager and R. de Dear, "Climate, comfort & natural ventilation: a new adaptive comfort standard for ASHRAE Standard 55," in Moving thermal comfort standards into the 21st century, 2001, [Online]. Available: http://www.escholarship.org/uc/item/2048t8nn.
[54] HMSO, Building Regulations 1991 L1: conservation of fuel and power, 1995 edition. 1995.
[55] HM Government, Building Regulations 2000 L1A: conservation of fuel and power in new dwellings, 2010 edition. UK, 2010.
[56] HM Government, Building Regulations 2010 L1A: conservation of fuel and power in new dwellings, 2013 edition with 2016 amendments. 2018.
[57] M. Li, "The Economical Operation of Coal Chain Grate Boiler," in IOP Conference Series: Earth and Environmental Science, 2018, doi: 10.1088/1755-1315/170/4/042056.
[58] M. Qu, O. Abdelaziz, H. Yin, New configurations of a heat recovery absorption heat pump integrated with a natural gas boiler for boiler efficiency improvement, Energy Convers. Manage. 87 (2014) 175–184, https://doi.org/10.1016/j.enconman.2014.06.083.
[59] L. Jiang, X. Ou, L. Ma, Z. Li, W. Ni, Life-cycle GHG emission factors of final energy in China, Energy Procedia 37 (2013) 2848–2855, https://doi.org/10.1016/j.egypro.2013.06.170.
[60] D. Che, Y. Liu, C. Gao, Evaluation of retrofitting a conventional natural gas fired boiler into a condensing boiler, Energy Convers. Manage. 45 (20) (2004) 3251–3266, https://doi.org/10.1016/j.enconman.2004.01.004.
[61] JGJ26, Design Standard for Energy Efficiency of Residential Buildings in Severe Cold and Cold Zones. 2010.